JGP Journal of General Physiology

RESEARCH ARTICLE

Duplex signaling by CaM and Stac3 enhances $Ca_V1.1$ function and provides insights into congenital myopathy

Jacqueline Niu[1], Wanjun Yang[1], David T. Yue, Takanari Inoue[1,2,3], and Manu Ben-Johny[4]

$Ca_V1.1$ is essential for skeletal muscle excitation–contraction coupling. Its functional expression is tuned by numerous regulatory proteins, yet underlying modulatory mechanisms remain ambiguous as $Ca_V1.1$ fails to function in heterologous systems. In this study, by dissecting channel trafficking versus gating, we evaluated the requirements for functional $Ca_V1.1$ in heterologous systems. Although coexpression of the auxiliary β subunit is sufficient for surface–membrane localization, this baseline trafficking is weak, and channels elicit a diminished open probability. The regulatory proteins calmodulin and stac3 independently enhance channel trafficking and gating via their interaction with the $Ca_V1.1$ carboxy terminus. Myopathic stac3 mutations weaken channel binding and diminish trafficking. Our findings demonstrate that multiple regulatory proteins orchestrate $Ca_V1.1$ function via duplex mechanisms. Our work also furnishes insights into the pathophysiology of stac3-associated congenital myopathy and reveals novel avenues for pharmacological intervention.

Introduction

Central to excitation–contraction (EC) coupling in skeletal muscle, $Ca_V1.1$ is an L-type voltage-gated calcium (Ca^{2+}) channel that senses transmembrane depolarization to initiate Ca^{2+} release from the SR RYR1 (Schneider and Chandler, 1973; Bannister and Beam, 2013). Although its cardiac counterpart $Ca_V1.2$ communicates with RYR2 via freely diffusing Ca^{2+} ions, $Ca_V1.1$ is conformationally coupled to RYR1, obviating the intermediary second messenger (Armstrong et al., 1972; Tanabe et al., 1990a; Ríos et al., 1992). This intimate physical linkage warrants a precise geometric arrangement of the two partners in the skeletal myotube: four $Ca_V1.1$s, termed tetrads, are disposed in ordered arrays that parallel RYR1 arrays at the surface–membrane/SR (peripheral-couplings) or tubular-membrane/SR (triad) interfaces (Franzini-Armstrong and Jorgensen, 1994; Lamb, 2000).

Fitting with this physiology, a cohort of auxiliary subunits such as β_{1A} (Schredelseker et al., 2009), $\alpha_2\delta$ (Obermair et al., 2005), γ_1 (Freise et al., 2000), and various SR proteins including RYR1 (Nakai et al., 1996; Avila and Dirksen, 2000; Bannister et al., 2016), JP45 (Anderson et al., 2006), and junctophilin (Golini et al., 2011) tune $Ca_V1.1$ function. To identify essential signaling partners, a top-down approach using primary cultures of skeletal myotubes obtained from gene knockout (KO) models (Obermair et al., 2008) and cell lines derived from dysgenic and normal myotubes have been insightful (Powell et al., 1996). However, such analyses have often revealed overlapping functions whereby loss of a single protein dramatically alters $Ca_V1.1$ localization and/or gating to ultimately disrupt EC coupling. These effects may be either direct or indirect depending on other proteins present in the complex. Thus, quantifying the role of a given modulator on $Ca_V1.1$ and the underlying regulatory mechanism is challenging. Intriguingly, recent studies have revealed that both calmodulin (CaM; Ohrtman et al., 2008; Stroffekova, 2008) and stac3 regulate $Ca_V1.1$, although underlying mechanisms remain to be fully elucidated (Horstick et al., 2013; Polster et al., 2015; Linsley et al., 2017a).

The Ca^{2+}-binding protein CaM has emerged as a dynamic regulator of neuronal and cardiac Ca^{2+} channels ($Ca_V1.2/3/4$ and $Ca_V2.1/2/3$; Halling et al., 2006; Minor and Findeisen, 2010; Ben-Johny et al., 2015). The binding of Ca^{2+}-free CaM (apoCaM) up-regulates the baseline open probability (P_O), whereas Ca^{2+}–CaM interaction relieves this initial enhancement manifesting as Ca^{2+}-dependent inactivation (CDI; Adams et al., 2014). For $Ca_V1.1$, however, CaM regulation has evaded consensus. Exogenously expressed CaM localizes to the skeletal muscle triad (Rodney and Schneider, 2003). CaM interaction with $Ca_V1.1$ has been controversial in biochemical studies, however, with some reporting

[1]Department of Biomedical Engineering, Johns Hopkins University, Baltimore, MD; [2]Department of Cell Biology, Johns Hopkins University, Baltimore, MD; [3]Center for Cell Dynamics, Institute for Basic Biomedical Sciences, Johns Hopkins University, Baltimore, MD; [4]Department of Physiology and Cellular Biophysics, Columbia University, New York, NY.

D.T. Yue died on 12/23/2014; Correspondence to Takanari Inoue: jctinoue@jhmi.edu; Manu Ben-Johny: mbj2124@cumc.columbia.edu.

weak to no binding (Ohrtman et al., 2008), whereas in vitro surface plasmon resonance measurements and crystallographic analysis suggest a high-affinity interaction with the channel carboxy tail (CT) in the presence of Ca^{2+} (Sencer et al., 2001; Black et al., 2005; Halling et al., 2009). Similarly, functional analysis of $Ca_V1.1$ in skeletal myotubes has revealed the ultra-slow and variable extent of CDI, casting doubt as to whether CaM is relevant for $Ca_V1.1$ function (Tanabe et al., 1990b; Ohrtman et al., 2008; Stroffekova, 2008). Interestingly, mutations of the CaM binding interface in the $Ca_V1.1$ CT strongly reduce EC coupling (Stroffekova, 2011).

Likewise, stac3 was recently identified as a component of the EC coupling machinery in association with debilitating congenital human myopathies (Stamm et al., 2008; Horstick et al., 2013; Nelson et al., 2013; Grzybowski et al., 2017). This autosomal-recessive disease was identified in a culturally isolated population of Native Americans (Stamm et al., 2008) but has since been observed in Middle Eastern, African, and South American individuals (Grzybowski et al., 2017; Telegrafi et al., 2017). Patients present with symptoms of muscle weakness, including short stature, kyphoscoliosis, talipes deformities, and drooping facial features, and increased susceptibility to malignant hyperthermia (Stamm et al., 2008; Grzybowski et al., 2017; Telegrafi et al., 2017). Functionally, homozygous KO of stac3 in mouse and zebrafish models led to markedly diminished $Ca_V1.1$ surface–membrane trafficking, reduced tetrad formation, loss of retrograde signaling, and a near-complete loss of EC coupling (Horstick et al., 2013; Nelson et al., 2013; Polster et al., 2015, 2016; Linsley et al., 2017a,b). However, overexpression of a myopathy-associated mutant stac3 partially rescued channel trafficking, although EC coupling remained reduced (Polster et al., 2016; Linsley et al., 2017a). Moreover, the structural determinants of $Ca_V1.1$ that mediate stac binding also remain unknown (Campiglio and Flucher, 2017). Thus, stac3 may elicit multiple regulatory functions of $Ca_V1.1$ through direct interactions with the channel or mediated by other triadic proteins (Polster et al., 2016; Linsley et al., 2017a).

To resolve these complex channel-regulatory mechanisms, a bottom-up approach whereby the effects of individual signaling molecules on $Ca_V1.1$ gating and trafficking are probed in a simplified system without an elaborate SR or t-tubules would be greatly beneficial (Dascal et al., 1992; Polster et al., 2015; Perni et al., 2017). However, functional analysis of $Ca_V1.1$ and its modulation by various signaling molecules in nonmuscle cell systems remains challenging (Perez-Reyes et al., 1989; Dascal et al., 1992; Johnson et al., 1997; Polster et al., 2015). Although homologous $Ca_V1.2$, $Ca_V1.3$, and $Ca_V1.4$ all exhibit reliable surface–membrane trafficking in heterologous systems in the presence of $\alpha_2\delta$ and β auxiliary subunits (Mikami et al., 1989; Catterall, 2000; Xu and Lipscombe, 2001; McRory et al., 2004), $Ca_V1.1$ is thought to be retained in internal organelles (Polster et al., 2015; Linsley et al., 2017b). Countering this classical purview, however, a recent functional study demonstrated that the cytosolic adapter protein stac3 with the $\alpha_2\delta/\beta$ subunits enabled $Ca_V1.1$ expression in human-derived tsA201 cells (Polster et al., 2015). Further analysis suggested that additional factors including the transmembrane γ_1 subunit may also permit $Ca_V1.1$ expression in tsA201 cells (Polster et al., 2016). The contrasting molecular requirements that permit $Ca_V1.1$ expression in heterologous systems obfuscate general principles that underlie channel trafficking and preclude systematic analysis of channel gating.

In this study, using a combination of whole-cell electrophysiology, FRET two-hybrid binding assay, and external-epitope labeling with flow cytometry (Yang et al., 2010), we demonstrate that $Ca_V1.1$, in fact, traffics to the plasma membrane of recombinant cell systems in the presence of auxiliary $\alpha_2\delta$ and β subunits alone. However, this baseline expression is lower than that for homologous L-type channels. Moreover, electrophysiological analysis reveals tiny ionic currents, suggesting that $Ca_V1.1$ has a low baseline P_O. Both CaM and stac3 enhance both surface–membrane trafficking and baseline P_O of $Ca_V1.1$. Moreover, we demonstrate that stac3 binds to the CT of $Ca_V1.1$, and stac3 mutations associated with congenital myopathy weaken this interaction, resulting in reduced channel surface–membrane trafficking. Delivery of CaM to the channel complex can partially reverse this trafficking defect. Interestingly, long-term application of small-molecule Ca_V modulators diltiazem and verapamil yields a partial rescue of channel trafficking. These results highlight the utility of reconstituted $Ca_V1.1$ in HEK293 cells as a simplified platform to distinguish regulatory effects of individual triadic signaling molecules. Additionally, the flow cytometric analysis of plasmalemmal expression may be an attractive venue for high-throughput screens of small molecules that modulate Ca_V trafficking. In all, our findings illustrate parallel signaling mechanisms that tune $Ca_V1.1$ trafficking and gating and shed light on pathophysiological mechanisms for stac3-associated congenital myopathies.

Materials and methods

Molecular biology

$Ca_V1.3_S$ was unmodified from previously published rat $Ca_V1.3_\Delta$ (GenBank Accession No. AF370009.1; Liu et al., 2010). GFP-$Ca_V1.1$ was a gift from Kurt Beam (University of Colorado at Denver, Denver, CO). Stac3 human isoform 2 was purchased from Origene. RYR1 P2 domain was synthesized by Genscript (sequence in Table S1). $Ca_V1.1$ CT chimeras were generated by first using PCR amplification with primers P01 and P02 (primers listed in Table S1) and restriction enzyme cutting sites XhoI and KpnI to generate a silent mutation to create a unique XbaI site ∼1–2 aa upstream of the EF hand and add an MssI restriction enzyme cutting site. $Ca_V1.3$ CI region was added to this construct by PCR amplification (P03 and P04) and inserted via XbaI and MssI restriction enzyme cutting sites. The $Ca_V1.1$ variant was generated by PCR amplification (P05 and P06) and cutting sites BglII–KpnI to insert an XbaI cutting site in place of the stop codon. Then, glycine-(12)-CaM_{WT} was PCR amplified (P07 and P08) and inserted into stopless $Ca_V1.1$ with XbaI and KpnI. $Ca_V1.1_{\Delta CT}$ was ordered from Genscript with the CT truncated after residue 1,397 (i.e., SILGPH*) and inserted with XhoI and KpnI. $Ca_V1.1$ (BBS) was generated by overlap PCR (P09–P12) and restriction enzyme sites SalI–XhoI to insert BBS. β_{2A}-glycine-(8)-CaM_{WT} was unchanged from previously published rat β_{2A} modifications (Yang et al., 2014). Using PCR amplification, we cloned CaM_{1234} (P08 and P13) into NotI–BsrGI to

generate β_{2A}-glycine-(8)-CaM_{1234}. β_{2A}-glycine-(12)-RYR1 P2 was generated from PCR amplification (P14 and P15) and inserted into β_{2A}-glycine-(32)-CaM_{WT} from a previously published construct (Sang et al., 2016) with BsrGI and compatible ends NheI–XbaI. C1 of stac3 was PCR amplified (P16 and P17) and cloned into pcDNA3 with NheI and BsrGI. Native American myopathy mutation was generated by QuikChange mutagenesis (P18 and P19). Venus- and Cerulean-tagged constructs were generated by PCR amplification (P20–P23) and inserted via NotI and XbaI restriction enzyme cutting sites into previously published constructs (Sang et al., 2016). All constructs were verified with DNA sequencing.

Transfection of HEK293 cells

For whole-cell electrophysiology, HEK293 cells were cultured on glass coverslips in 10-cm dishes and transfected using a calcium phosphate method (Peterson et al., 1999) with the following DNA combinations: 8 µg α_1 subunit of Ca^{2+} channel, 8 µg rat β_{2A} (GenBank Accession No. M80545; Perez-Reyes et al., 1992) or β_{1A} from mouse (NP112450.1), and 8 µg rat $\alpha_2\delta$ (NM012919.2; Tomlinson et al., 1993). 3 µg SV40 T antigen was also cotransfected to enhance expression, and 8 µg CaM variants, stac3 variants, and RYR1 P2 variants were transfected for overexpression of trafficking agent. Similarly, for bungarotoxin labeling, HEK293 cells were cultured in 60-mm dishes and transfected by calcium phosphate precipitation. DNA concentration used was half that for electrophysiology conditions.

For FRET two-hybrid experiments, HEK293 cells were cultured on glass-bottom dishes and transfected using a standard polyethylenimine protocol (Lambert et al., 1996). Epifluorescence was collected 1–2 d after transfection.

For the drug study, drugs were purchased from Sigma-Aldrich. Nifedipine and diltiazem were diluted to 1 mM in DMSO, and verapamil, ranolazine, and mexiletine were diluted to 10 mM in DMSO before being added to cell culture media. Cells were incubated in the respective concentration of drugs for 24 h before bungarotoxin labeling.

Whole-cell electrophysiology

Whole-cell electrophysiology was performed at room temperature 1–4 d after transfection with Axopatch 200A (Axon Instruments). Glass pipettes were made from borosilicate glass (BF150-86-10; Sutter Instrument) at 1–3 MΩ resistance with a horizontal puller (P-97; Sutter Instrument) and fire polisher (microforge; Narishige). We low-pass filtered recordings at 2 kHz, sampled at 10 kHz, and used P/8 leak subtraction with 70% series resistance and capacitance compensation. Internal solution contained (in mM): $CsMeSO_3$ 114, $CsCl_2$ 5, $MgCl_2$ 1, MgATP 4, HEPES 10, and 1,2-bis(o-aminophenoxy)ethane-N,N,N′,N′-tetraacetic acid 10, adjusted to 295 mOsm with CsMeSO3 and pH 7.4 with CsOH. External solution contained (in mM): TEA-MeSO3 140, HEPES 10, and CaCl2 40, adjusted to 300 mOsm with TEA-$MeSO_3$ and pH 7.4 with TEA-OH. For measuring charge movements, we added 0.2 mM $LaCl_3$ and 1.0 mM $CdCl_2$ to the external solution. We used a holding potential of −80 mV, family of test pulses from −30 mV to +80 mV in 10-mV increments, and repetition interval of 20 s for all whole-cell recordings. Custom MATLAB (MathWorks) software was used to determine peak current, and mean peak current densities are plotted with SEM.

Peak current density–voltage curves were fitted with the following equation:

$$J_{peak} = G_{max}(V - V_{rev})/\{1 - \exp[-(V - V_{1/2})/k_G]\}, \quad (1)$$

where J_{peak} is the peak current density at test potential V, G_{max} is maximal channel conductance, V_{rev} is the reversal potential, $V_{1/2}$ is the half-activation voltage, and k_G is the slope factor (Table S2).

Normalized gating charge–voltage curves were fitted with the following equation:

$$Q_{norm} = Q_{max} \cdot \left\{ \frac{f}{1 + \exp[-(V - V_{1/2,a})/SF_a]} + \frac{1 - f}{1 + \exp[-(V - V_{1/2,b})/SF_b]} \right\}, \quad (2)$$

where Q_{norm} is the gating charge movement at voltage V normalized to value at +80 mV. Gating charge movement is composed of a double Boltzmann relation, with Q_{max} as saturating normalized gating charge; $V_{1/2.a}$ and $V_{1/2.b}$ are half-activating potentials for the two components; and SF_a and SF_b are slope factors for the two components.

FRET two-hybrid assay

Three-cube FRET fluorescence of transfected HEK293 cells was measured on an inverted fluorescence microscope in 2 mM Ca^{2+} Tyrode's under resting Ca^{2+} intracellular concentrations and 10 mM Ca^{2+} Tyrode's incubated with 4 µM ionomycin (Sigma-Aldrich) under Ca^{2+}/CaM conditions. Different concentrations and ratios of DNA were transfected to achieve a range of donor molecule (D_{free}) concentrations. FRET efficiency (E_A) for each individual cell was calculated (Erickson et al., 2001), and effective dissociation constants ($K_{d,EFF}$) were computed by fitting the binding curve $E_A = [D_{free}]/(K_{d,EFF} + [D_{free}]) \cdot E_{A,max}$ iteratively. For stac3 Native American myopathy constructs where plateaus of FRET binding curves were not clearly defined by data, we assumed that stac3 adopts the same conformation and possesses the same $E_{A,max}$ (Ben Johny et al., 2013).

Bungarotoxin labeling assay

First, we washed transfected cells twice with DPBS (with Mg^{2+} and Ca^{2+}; MediaTech). Then, we blocked nonspecific binding sites with 3% BSA/DMEM for 30 min at room temperature. We incubated cells with 1 µM α-bungarotoxin-biotin (Invitrogen) in 3% BSA/DMEM for 1 h at room temperature in the dark. On ice and in the dark, cells were washed twice with DPBS, incubated three times for 5 min with DPBS, and incubated for 1 h with 10 nM Qdot655 for flow cytometry or Qdot605 for confocal imaging (Invitrogen) in 3% BSA/DMEM. Finally, cells were washed with DPBS and imaged on the confocal microscope in 2 mM Ca^{2+} Tyrode's or harvested with trypsin, washed with PBS (without Mg^{2+} and Ca^{2+}), and resuspended for flow cytometry.

The total GFP fluorescence is proportional to the number of channels in a cell,

$$S_G = N_{tot} \cdot \alpha_G \cdot I_0, \quad (3)$$

where α_G corresponds with the brightness of single GFP given the imaging setup, and I_0 is the intensity of the excitation lamp. Similarly, the number of channels at the plasma membrane is given by

$$S_R = N_{surface} \cdot (4 \cdot \alpha_R) \cdot I_0 \cdot \varepsilon, \quad (4)$$

where α_R corresponds with the brightness of a single quantum dot (QD) molecule when assessed through our imaging setup, I_0 is the intensity of the excitation lamp, and 4 corresponds with the stoichiometry for biotin–streptavidin interaction. The factor ε is the efficiency of QD labeling. The ratio of the two equations yields Eq. 5 and is proportional to the fraction of surface-membrane channels.

Confocal optical imaging

We captured exemplar images of bungarotoxin-labeled HEK cells with the Olympus FluoView FV300 confocal laser scanning microscope and FluoView software (Olympus). Using the Olympus Plan Apochromat 403 or 603 oil objective (NA 1.40, PLAPO60XO3; Olympus), GFP was excited with an argon laser (488 nm), and Qdot-605 streptavidin conjugate (Invitrogen) was excited with a helium neon (HeNe) green laser. Olympus optical filters used include 442/515-nm excitation splitter (FV-FCV), 570-nm emission splitter (FV-570CH), BA510 immunofluorescence and BA530RIF for GFP emission channel, and 605BP filter for Qdot channel. Images were converted and merged in ImageJ (National Institutes of Health).

Flow cytometry

Fluorescence of harvested cells was measured with an Attune acoustic focusing flow cytometer (Life Technologies) in high-sensitivity mode with a flow rate of 100 µl/min. We used the blue (488 nm) laser to excite GFP and Qdot to collect green and red fluorescence, respectively. Green fluorescence was measured through the 574/26 optical filter. Likewise, red fluorescence was measured through the 640LP optical filter. Flow cytometer was calibrated and maintained as previously published (Lee et al., 2016). Control experiments included untransfected cells, GFP-only cells, cells transfected with $Ca_V1.1$ and stac3 as a negative control, and cells with $CaV1.1_{BBS}$ and stac3 as a positive control. Data were exported as FCS files and analyzed with custom MATLAB software.

Data processing and statistical analysis

Raw data were gated by forward- and side-scatter signals to filter for single and healthy cells, and green signals >1.5×10^5 units were excluded because of nonlinearities in flow cytometer measurements (Lee et al., 2016). Red signals >2×10^5 units were excluded because of PMT saturation and accounted for <1% of total collected points. To correct for the true green (S_G) and red (S_R) signals, we averaged red signal ($\hat{S}_{R,blank}$) and green signal ($\hat{S}_{G,blank}$) of blank cells. We also calculated the slope for GFP bleed-through into the red channel ($f_{RED,GFP}$) to be ∼2.65% because of the broadness of the GFP emission spectrum, yielding two equations: $S_G = \hat{S}_G - \hat{S}_{G,blank}$ and $\hat{S}_R = S_R - \hat{S}_{R,blank} - f_{RED,GFP} \cdot S_G$, where $\hat{S}_G$ is the raw green signal and S_{RED} is the red signal. Welch's t test was used to statistically compare two trafficking conditions, and P values report the probability for the null hypothesis that the respective ϕ_{max} for conditions compared are equal. To ensure robustness, we also used a rank-sum test. In all cases, the P value for rank-sum test was similar to that with Welch's t test. The number of independent trials and total number of cells analyzed are listed in Table S3.

Online supplemental material

The supplemental text explicitly derives the Langmuir relationship between plasmalemmal trafficking and affinity of binding for stac3 pertaining to Fig. 7 l. Fig. S1 shows individual peak current densities from individual cells pertaining to Fig. 1. Fig. S2 shows additional trafficking data and electrophysiological parameters for $Ca_V1.1$ channels in the presence of β_{2A} subunit alone Fig. 6 a. Fig. S3 shows additional justification for distinct interfaces for CaM versus stac3 within $Ca_V1.1$. Fig. S4 shows extended data with the extent of enhancement in trafficking of $Ca_V1.1$ in the presence of pharmacological chaperones. Table S1 lists primers used. Table S2 summarizes electrophysiological parameters pertaining to Fig. 1. Table S3 provides supplemental information for trafficking experiments including sample size.

Results

Functional determinants for expression of $Ca_V1.1$ in heterologous systems

In comparison with other L-type Ca channels, $Ca_V1.1$ expresses poorly in heterologous cell systems (Perez-Reyes et al., 1989; Polster et al., 2015). Fig. 1 a shows an exemplar inward Ca^{2+} current elicited in response to a voltage-step depolarization from a HEK293 cell transiently expressing $Ca_V1.3$ pore-forming α_1 subunit with auxiliary β_{2A} and $\alpha_2\delta$ subunits. Population data of mean peak current densities elicited in response to a family of step depolarizations further illustrate robust expression of $Ca_V1.3$ in HEK293 cells (Fig. 1 a). In contrast, when $Ca_V1.1$ α_1 subunit is coexpressed with both β_{2A} and $\alpha_2\delta$ auxiliary subunits, we observe minimal ionic currents (Figs. 1 b and S1). Given the functional difference between $Ca_V1.1$ and $Ca_V1.3$ despite their overall structural similarity, we sought to identify requirements for functional expression of $Ca_V1.1$ in heterologous systems.

First, we reasoned that the Ca_V channel cytoplasmic domains may contain critical motifs that differentially enhance channel function (Fang and Colecraft, 2011). In this regard, for related $Na_V1.9$ sodium channels that also fail to express in nonexcitable cells, a chimeric approach that replaced the CT of $Na_V1.9$ with that from $Na_V1.4$ yielded robust currents (Goral et al., 2015). Paralleling this approach, we exchanged the CT of $Ca_V1.1$ α_1 subunit with that of $Ca_V1.3$. Electrophysiological analysis revealed robust currents for the chimeric channels (Fig. 1 c), suggesting that the CT is a key determinant for functional expression.

Second, key $Ca_V1.1$-interacting proteins may modulate channel function by either serving as chaperones to promote plasmalemmal trafficking or enhancing channel activity. Indeed, recent research shows that $Ca_V1.1$ currents can be reestablished in HEK293 cell systems by coexpression of stac3, an adapter protein essential for skeletal muscle function (Polster et al., 2015). Exemplar current trace and population data of $Ca_V1.1$ after coexpression of stac3 in HEK293 cells further confirm these findings

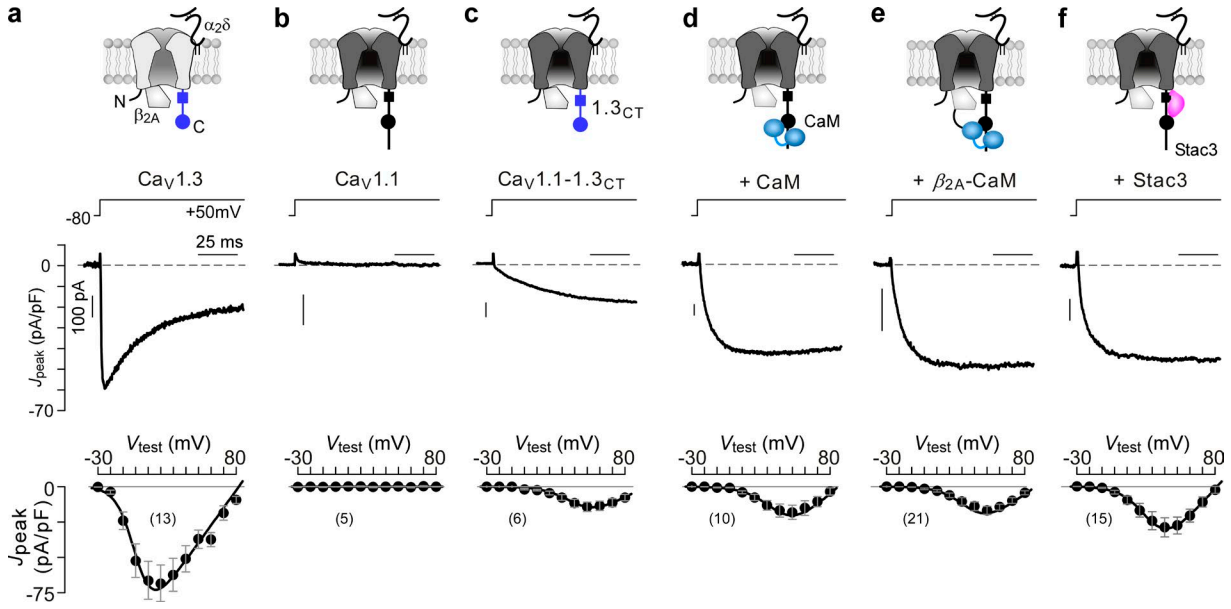

Figure 1. **Robust expression of $Ca_V1.1$ is dependent on its CT. (a)** $Ca_V1.3$ with β_{2a} and $\alpha_2\delta$ auxiliary subunits exhibits robust currents in HEK293 cells. Top: Cartoon depicts the $Ca_V1.3$ pore-forming α_1 subunit with auxiliary subunits cotransfected. Middle: Exemplar current traces in response to a voltage-step protocol from −80 mV to +50 mV. Gray dashed line, baseline of 0 pA. Bottom: Population data for current density–voltage relationship from −30 to +80 mV in 10-mV increments for indicated number of cells (*n*). Error bars show mean ± SEM. Gray solid line, baseline of 0 pA. **(b)** $Ca_V1.1$ with auxiliary subunits exhibits minimal ionic currents. Format as in a. **(c)** Chimeric $Ca_V1.1$ with the $Ca_V1.3$ CT partially rescues functional expression. Format as in a. **(d)** Coexpression of stac3 also elicits robust Ca^{2+} currents through $Ca_V1.1$. Format as in a. **(e and f)** Restoration of CaM to $Ca_V1.1$ through overexpression of CaM or direct linkage to the auxiliary β_{2A} subunit produces robust functional expression. Format as in a.

(Fig. 1 d). As CaM is a canonical interacting partner for the CT of various Ca_Vs, we reasoned that CaM might also permit functional expression of $Ca_V1.1$. Indeed, overexpression of CaM alone (Fig. 1 e) or localization of CaM to the $Ca_V1.1$ complex via fusion to β_{2A} subunit (Fig. 1 f) reveals a marked enhancement in Ca^{2+} currents. Thus, multiple seemingly disparate manipulations permit $Ca_V1.1$ expression in nonexcitable cells.

$Ca_V1.1$ exhibits reduced baseline plasmalemmal trafficking

Thus informed, we sought to dissect molecular mechanisms that enable $Ca_V1.1$ function in HEK293 cells. The functional expression of ion channels may be enhanced from changes in three vital parameters: (1) the number of channels at the surface membrane dictated by protein trafficking, (2) ion permeation, and (3) channel gating.

To quantify the relative fraction of channels at the cell surface membrane, we used a dual-labeling approach (Yang et al., 2010) whereby the α_1 subunit is tagged with both a GFP on the cytoplasmic amino terminus and an external epitope composed of a 13-aa α-bungarotoxin–binding site (BBS) inserted into the extracellular loop between transmembrane segments 5 and 6 (S5 and S6) of domain II (Fig. 2 a, $Ca_V1.1_{BBS}$). To label surface membrane channels, we incubated cells with cell-impermeable biotin-conjugated α-bungarotoxin and visualized using streptavidin covalently attached to a red QD; the total expression of $Ca_V1.1$ in a cell is determined by monitoring the GFP fluorescence (Sekine-Aizawa and Huganir, 2004). The high affinity and specificity of bungarotoxin for the BBS site facilitates reliable detection of surface-membrane $Ca_V1.1$ with minimal background fluorescence (Sekine-Aizawa and Huganir, 2004). We first verified the functionality of $Ca_V1.1_{BBS}$ by cotransfecting β_{2a}-CaM_{WT} into HEK cells. The resultant Ca^{2+} currents exhibited properties comparable with those of unmodified $Ca_V1.1$ (Fig. 2 a). We probed baseline plasmalemmal expression for $Ca_V1.1_{BBS}$ in the presence of β_{2A} and $\alpha_2\delta$ subunits using confocal imaging (Fig. 2 b). The left subpanel shows the transmitted light image of an exemplar cell, and the middle subpanels show green (S_G) and red (S_R) fluorescence images indicating GFP from total channels and QD emissions from extracellular channels, respectively. The far-right merged image showcases the difference in intracellular and extracellular labeling of $Ca_V1.1_{BBS}$. Although strong GFP fluorescence is evident, external QD labeling is sparse, indicating poor surface–membrane expression of $Ca_V1.1$ (Fig. 2 b). That said, we did observe some surface–membrane labeling in a few cells, suggesting that $Ca_V1.1$ with just $\alpha_2\delta$ and β subunits might be sufficient for surface–membrane trafficking, albeit with a lower efficacy. Analysis of external epitope labeling from a multitude of individual cells would help resolve such ambiguities.

Accordingly, we used flow cytometric analysis to quantify surface–membrane trafficking at the population level by determining the total GFP (S_G) and QD (S_R) fluorescence from individual cells. For a given cell, the ratio of red to green fluorescence ($\phi = S_R/S_G$) is proportional to the fraction of surface–membrane channels (f_{mem}) and serves as a quantifiable metric for trafficking efficacy:

$$\frac{N_{surface}}{N_{tot}}\frac{4\cdot\alpha_R\cdot\varepsilon}{\alpha_G} = f_{mem}\cdot\frac{4\cdot\alpha_R\cdot\varepsilon}{\alpha_G}. \quad (5)$$

The factors α_R and α_G are brightness of single QD and GFP fluorophores, respectively, and ε is the efficiency of labeling. Given this framework, we plotted S_R versus S_G obtained from individual

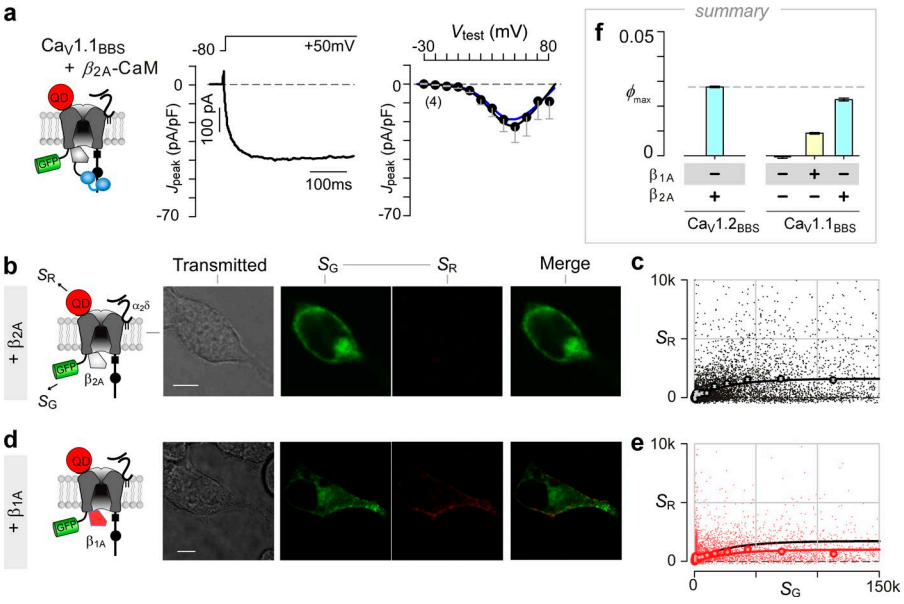

Figure 2. **Quantifying $Ca_V1.1$ surface–membrane trafficking using a dual-labeling approach. (a)** Top: To label surface–membrane $Ca_V1.1$ channels, we inserted BBS into the domain II S5–S6 linker and a GFP to the amino terminus yielding $Ca_V1.1_{BBS}$. Middle: $Ca_V1.1_{BBS}$ yields robust Ca^{2+} currents when coexpressed with β_{2A}-CaM. Exemplar trace shows Ca^{2+} current elicited with a +50-mV voltage-step. Right: J_{peak} (mean ± SEM) computed from indicated number of cells (n). Blue relation shows J_{peak} relationship for WT $Ca_V1.1$. **(b)** $Ca_V1.1$ in the presence of $\alpha_2\delta$ and β_{2A} auxiliary subunits traffics poorly and exhibits weak extracellular labeling. Left: Schematic shows external-epitope labeling of GFP-tagged $Ca_V1.1_{BBS}$ in the presence of $\alpha_2\delta$ and β_{2A} auxiliary subunits. In this figure, the external epitope is α-bungarotoxin conjugated to QD. Right: Transmitted-light, intracellular GFP (S_G), extracellular QD (S_R), and merged images for transfected and labeled cells were collected by confocal microscopy. Bars, 5 µm. **(c)** Flow-cytometric analysis confirms weak surface–membrane expression for $Ca_V1.1_{BBS}$ with $\alpha_2\delta$ and β_{2A} auxiliary subunits cotransfected. QD fluorescence, S_R, is plotted as a function of GFP fluorescence, S_G. Each dot represents one cell. Black dashed line indicates no extracellular labeling ($S_R = 0$). Black circles and fit denote binned data for QD and GFP fluorescence fitted to a single-exponential function. **(d and e)** $Ca_V1.1_{BBS}$ coexpressed with auxiliary β_{1A} and $\alpha_2\delta$ subunits traffic to the plasma membrane. Format as in b and c. **(f)** Bar graph summarizes saturating surface–membrane trafficking limit ϕ_{max}, proportional to the maximal fraction of $Ca_V1.1$ trafficked to the plasma membrane under various conditions. $Ca_V1.1$ fails to exhibit plasmalemmal trafficking in the absence of β subunits. In the presence of either β_{1A} or β_{2A}, $Ca_V1.1$ exhibits detectible baseline trafficking, albeit reduced in comparison with $Ca_V1.2$.

cells expressing $Ca_V1.1_{BBS}$ with β_{2A} and $\alpha_2\delta$ subunits after 1 d of transfection (Fig. 2 c). Consistent with confocal imaging data, flow-cytometric analysis showed a mixed population of cells: one fraction exhibited minimal surface–membrane labeling ($S_R = 0$), and the other demonstrated reliable QD labeling ($S_R > 0$). Binned data reveal a saturating relationship for S_R as S_G increases, with a maximal value of ~1,923 ± 51 fluorescence units. We estimated the saturating surface–membrane trafficking limit (ϕ_{max}) as the mean ratio ϕ for individual cells exhibiting high GFP fluorescence (i.e., $5.4 \times 10^4 \le S_G \le 1.4 \times 10^5$) to be 0.0225 ± 0.0006 (Fig. 2 f). We excluded values >1.4×10^5 GFP fluorescence units because of previously identified nonlinearities in fluorescence measurements from our flow cytometer above this value (Lee et al., 2016). In comparison, ϕ_{max} for $Ca_V1.2_{BBS}$ is ~0.0276 ± 0.0004 (Fig. 2 f). Similarly, coexpression of $Ca_V1.1_{BBS}$ with β_{1A} subunit that is endogenous to skeletal myotubes also resulted in weak but detectible QD labeling based on confocal imaging (Fig. 2 d) and population analysis (Fig. 2, e and f). In contrast, $Ca_V1.1_{BBS}$ exhibited minimal plasmalemmal expression in the absence of β subunits (Fig. 2 f). These findings further demonstrate that β and $\alpha_2\delta$ subunits are sufficient for plasmalemmal trafficking of $Ca_V1.1$ in nonexcitable cells; however, this baseline trafficking efficacy is diminished in comparison with related Ca_V channels.

CaM and stac enhance $Ca_V1.1$ surface membrane trafficking

With baseline plasmalemmal expression levels established, we probed the effect of CaM and stac3 on overall $Ca_V1.1$ plasmalemmal trafficking. When CaM is delivered locally to $Ca_V1.1_{BBS}$ via β_{2A}-CaM, QD labeling is markedly enhanced, suggesting improved plasmalemmal localization (Fig. 3 a). Flow cytometric analysis of $Ca_V1.1$ coexpressed with β_{2A}-CaM revealed an overall enhancement in the QD labeling (Fig. 3, b and e) in comparison with levels with the β_{2A} subunit alone ($P < 10^{-5}$; Figs. 2 c and 3 e) or with β_{2A} fused to a sham payload, the P2 domain of RYR1 ($P < 10^{-5}$; Fig. 3 e). Likewise, the surface membrane expression of $Ca_V1.1$ bound to the skeletal muscle β_{1A} subunit was also enhanced significantly upon coexpression of CaM as a separate molecule ($P < 10^{-5}$; Fig. 3 f).

We next explored whether stac3, like CaM, enhances plasmalemmal trafficking of $Ca_V1.1$. Confocal imaging (Fig. 3 c) and flow cytometric analysis (Fig. 3 d) revealed substantial enhancement in QD labeling for $Ca_V1.1_{BBS}$ with stac3 in the presence of β_{2A} ($P < 10^{-5}$), consistent with improved channel trafficking. Similarly, stac3 enhanced $Ca_V1.1$ trafficking in the presence of β_{1A} subunit ($P < 10^{-5}$; Fig. 3 f). In contrast, coexpression of mutant stac3 containing only the C1 domain only partially enhanced surface–membrane trafficking ($P < 10^{-5}$; Fig. 3 f). Together, these results demonstrate that both CaM and stac3 enhance plasmalemmal trafficking of $Ca_V1.1$.

Molecular determinants for CaM and stac3-mediated enhancement of $Ca_V1.1$ trafficking

We next sought to identify key channel elements that mediate CaM- and stac3-dependent enhancement in $Ca_V1.1$ trafficking. As the carboxy terminus is critical for $Ca_V1.1$ functional expression, we tested the binding of CaM and stac3 to this channel domain (Fig. 4 a). Indeed, for nearly all $Ca_V1/2$ channels, CaM is a well-established partner for the CT known to modulate channel function (Peterson et al., 1999; Qin et al., 1999; Zühlke et al., 1999; Lee et al., 2000; Pitt et al., 2001; Liang et al., 2003; Singh et al., 2006; Yang et al., 2006). Consequently, we used a FRET two-hybrid binding assay (Erickson et al., 2001) in live cells to quantify CaM binding. We coexpressed cerulean-tagged CaM (Cer-CaM_{WT}) with

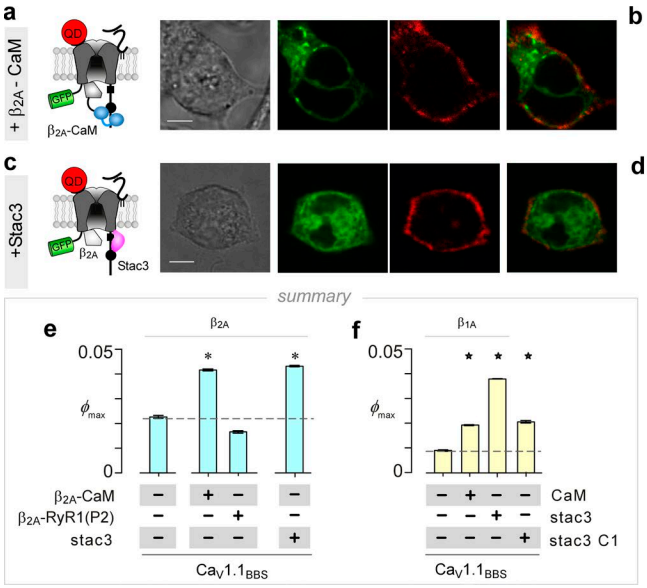

Figure 3. **CaM and Stac3 enhance surface–membrane trafficking of $Ca_V1.1$. (a and b)** Confocal imaging and flow cytometry show that cotransfection of β_{2a}-CaM augments $Ca_V1.1$ surface–membrane labeling. $\alpha_2\delta$ was cotransfected. Format as in Fig. 2 (b and c). Blue circles and fit in d correspond with binned data in the presence of β_{2a}-CaM, and black fit is the relation with β_{2A} reproduced from Fig. 2 c to facilitate comparison with baseline $Ca_V1.1$ trafficking. **(c and d)** Confocal imaging and flow cytometry of $Ca_V1.1_{BBS}$ cotransfected with stac3, β_{2A}, and $\alpha_2\delta$ subunits confirms enhanced surface–membrane trafficking of $Ca_V1.1$. Format as in Fig. 2 (b and c). Bars, 5 µm. **(e)** Bar graph summary shows marked enhancement in saturating surface–membrane trafficking limit ϕ_{max}, with coexpression of β_{2A}-CaM but not β_{2A} tethered to RYR1 P2 domain (β_{2A}-RYR1[P2]) in comparison with β_{2A} alone. Similarly, stac3 coexpression also enhances ϕ_{max}. **(f)** Bar graph summary illustrates enhancement in surface–membrane trafficking of $Ca_V1.1$ bound to β_{1A} subunit after coexpression of CaM or stac3 alone. *, $P < 10^{-5}$ with Welch's *t* test. Error bars show mean ± SEM.

Venus-tagged $Ca_V1.3$ CT, including the dual vestigial EF hands and the pre-IQ and IQ domains (Ven-$Ca_V1.3$ Ca^{2+} inactivation [CI]), and measured FRET efficiency (E_A) between the donor–acceptor pairs (Fig. 4 b). Strong binding of Cer-CaM_{WT} to Ven-$Ca_V1.3$ CI was observed under both basal and elevated Ca^{2+} conditions (Fig. 4 b), consistent with prior research (Ben Johny et al., 2013). In contrast, FRET two-hybrid analysis of Venus-tagged $Ca_V1.1$ CI (Ven-$Ca_V1.1$ CI) and Cer-CaM_{WT} showed weak binding under both basal and elevated Ca^{2+} conditions (Fig. 4 c). This weak affinity is consistent with a significant fraction of $Ca_V1.1$ lacking prebound CaM in endogenous conditions in HEK293 cells. In like manner, FRET two-hybrid analysis of Cer-tagged stac3 with Ven-$Ca_V1.1$ CI also revealed strong binding (Fig. 4 d), with $K_{d,EFF}$ ~12,000 D_{free} units ~400 nM. Fig. 4 e compares relative binding affinities for both CaM and stac3 with Ca_V CT obtained from FRET two-hybrid experiments. Altogether, these findings raise the possibility that the binding of CaM or stac3 to the $Ca_V1.1$ CT may be critical for its function.

Accordingly, we reasoned that the deletion of the CT would abrogate stac3- and CaM-mediated enhancement in $Ca_V1.1$ trafficking, a prediction that could be assessed readily using the flow cytometric assay. With β_{1A} and $\alpha_2\delta$ coexpressed, $Ca_V1.1(\Delta CT)_{BBS}$ with a truncated CT showed significant enhancement in trafficking in comparison with the WT channels ($P < 10^{-5}$; Fig. 4 f). However, coexpression of either β_{2A}-CaM ($P = 0.4$) or stac3 ($P = 0.11$) did not further enhance surface–membrane trafficking of $Ca_V1.1$ (Fig. 4 f). These results suggest that CaM and stac3 binding to the CT is functionally critical to enhance plasmalemmal trafficking. Moreover, FRET two-hybrid experiments in Fig. 4 c revealed that CaM binding affinity to the $Ca_V1.1$ CT was substantially enhanced in the presence of Ca^{2+}. Functionally, this difference in affinity would suggest that abrogating Ca^{2+}-binding to CaM would diminish CaM-dependent enhancement in $Ca_V1.1$ plasmalemmal trafficking. Indeed, coexpression of $Ca_V1.1_{BBS}$ with β_{2A} fused to a mutant CaM lacking Ca^{2+} binding (β_{2A}-CaM_{1234}) resulted in minimal enhancement in QD labeling (Fig. 4 g; $P < 10^{-5}$ for $Ca_V1.1$ with β_{2A}-CaM_{1234} compared with β_{2A}-CaM_{WT}). In all, these results suggest that the occupancy of $Ca_V1.1$ CT is closely linked to proper channel function, and an emerging repertoire of CT-binding proteins may modify Ca_V function via parallel mechanisms (Park et al., 2010; Wang et al., 2010; Marshall et al., 2011; Flynn and Altier, 2013; Hall et al., 2013).

Distinct binding sites on the CT allow CaM and stac3 to act independently

Given that both CaM and stac3 bind to the channel CT to enhance surface–membrane expression, we examined whether these agents act independently or through a shared endpoint. Consequently, to further delineate the CT binding interface for stac3 and CaM, we parsed the CT into three distinct segments: dual vestigial EF hands and pre-IQ and IQ domains. Using FRET two-hybrid assay, we probed binding between Venus-tagged channel segments and cerulean-tagged CaM or stac3. Ca^{2+}/CaM exhibits a markedly higher affinity to the pre-IQ and IQ domains in comparison with the dual vestigial EF hand segments (Fig. 5, a and b). In contrast, stac3 preferentially binds to the dual vestigial EF hand segments in comparison with the pre-IQ and IQ domains (Fig. 5, c and d). Importantly, these findings are in contrast with a recent study that suggested direct IQ binding based on reduced colocalization of $Ca_V1.1$ and stac3 after mutations in the IQ domain (Campiglio et al., 2018). In light of our present findings, it is possible that mutations in the IQ may indirectly alter stac3 interaction with upstream elements. In all, these findings demonstrate that stac3 and CaM prefer distinct CT interfaces.

Thus, we probed surface–membrane labeling of $Ca_V1.1_{BBS}$ in the presence of both β_{2A}-CaM and stac3. If the two agents act through a shared endpoint, then their combination will not further increase trafficking. However, flow cytometric analysis revealed that the two agents combinatorially enhance the trafficking of $Ca_V1.1_{BBS}$ nearly sixfold, suggesting that they act

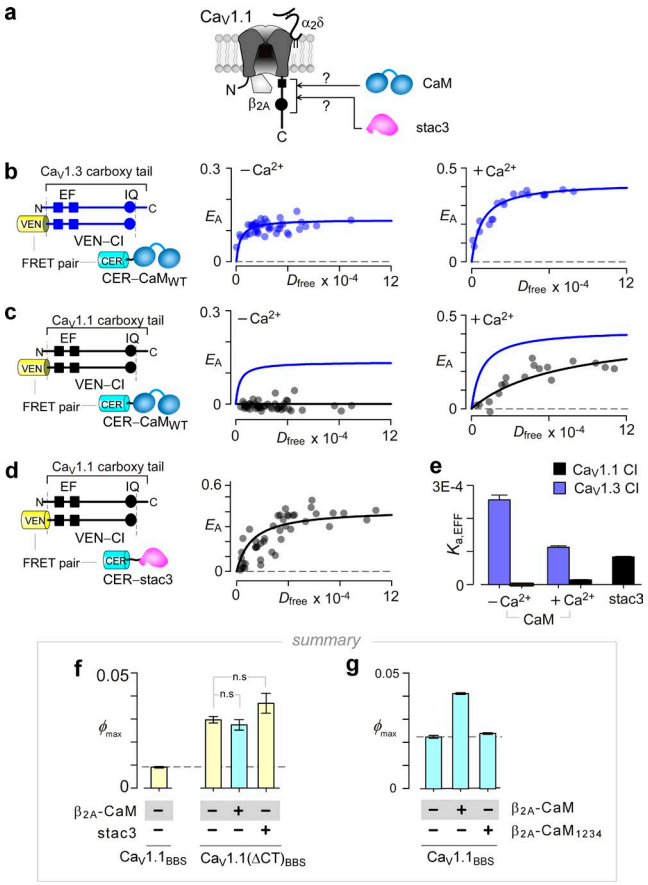

Figure 4. **$Ca_V1.1$ CI harbors CaM and stac3 and is critical for plasmalemmal trafficking. (a)** Cartoon schematic shows the potential interaction of $Ca_V1.1$ CI with CaM and stac3. **(b)** Left: Schematic shows FRET binding pairs, Cer-CaM_{WT} and Ven-$Ca_V1.3$ CI. The CI module consists of the dual vestigial EF hand and pre-IQ and IQ segments of the channel CT. Middle: The CI region of $Ca_V1.3$ binds with a high affinity to apoCaM ($K_{d,EFF}$ = 3,000 D_{free} units ~98 nM). FRET efficiency (E_A) is plotted as a function of donor fluorophore–tagged molecule (D_{free}) concentration (right). Gray dashed line indicates baseline for no binding. Right: $Ca_V1.3$ binds well to Ca^{2+}/CaM ($K_{d,EFF}$ = 8,000 D_{free} units ~260 nM). **(c)** In contrast, the CI region of $Ca_V1.1$ binds weakly to both apoCaM and Ca^{2+}/CaM ($K_{d,EFF}$ = 70,000 D_{free} units ~2.3 µM). Format as in b. **(d)** Stac3 binds with a high affinity to the CI region of $Ca_V1.1$ ($K_{d,EFF}$ ~12,000 D_{free} units ~400 nM). **(e)** Bar graph summarizes binding affinities from FRET curves (mean ± SEM). **(f)** Deletion of the entire $Ca_V1.1$ CT ($Ca_V1.1[\Delta CT]_{BBS}$) enhances baseline plasmalemmal trafficking. However, coexpression of β_{2A}-CaM or stac3 fails to enhance surface–membrane trafficking, suggesting that the CT is a critical determinant for channel trafficking. **(g)** Bar graph summary of ϕ_{max} shows that the increase in $Ca_V1.1$ plasmalemmal trafficking by CaM is Ca^{2+} dependent, consistent with differences in the binding of CaM to $Ca_V1.1$ CT (c).

independently through distinct sites on the CT ($P < 10^{-5}$; Fig. 5, e–g). In contrast, coexpression of freely diffusing CaM with $Ca_V1.1_{BBS}$ and β_{2A}-CaM did not further enhance trafficking (P = 0.13; Fig. 5 g), suggesting that the additive effect here did not result from incomplete saturation of channel CT by CaM. Together, these findings suggest that $Ca_V1.1$ plasmalemmal trafficking is enriched by a duplex signaling mechanism.

CaM and stac3 enhance the open probability of $Ca_V1.1$

With the role of CaM and stac3 on $Ca_V1.1$ trafficking established, we probed their effects on channel gating. However, as the activation of $Ca_V1.1$ is right-shifted to near its reversal potential (Table S2), detecting single-channel openings reliably in an on-cell configuration is challenging as the unitary currents at these voltages are small. Thus, to estimate changes in the maximal open probability, we analyzed macroscopic I_{tail} and overall gating charge movement. More specifically, the peak I_{tail} is linearly proportional to both the steady-state P_O of the channel at the activating prepulse potential and the number of surface–membrane channels. However, the total gating charge moved at the reversal potential (q_{rev}) is proportional to the number of surface–membrane channels. Gating charges can be isolated by blocking ion currents with heavy metals Cd^{2+}/La^{3+}. Thus, the ratio I_{tail}/q_{rev} is linearly proportional to P_O and serves as a convenient proxy to estimate changes in $P_{O,max}$ under various conditions.

Although our initial functional research failed to detect appreciable $Ca_V1.1$ currents with auxiliary β_{2A} and $\alpha_2\delta$ subunits coexpressed (Fig. 1 b), these experiments were conducted 1 d after transient transfection. Our trafficking research instead showed that $Ca_V1.1$ surface–membrane expression with the same subunits is substantially enhanced ($P < 10^{-5}$) several days after transient transfection (Fig. S2 a). As such, we conducted whole-cell patch-clamp experiments of $Ca_V1.1$ with auxiliary β_{2A} and $\alpha_2\delta$ subunits 2–4 d after transfection (Fig. S2 b). Scrutiny of current recordings revealed substantial gating currents in response to a 100-ms activating pulse to +80 mV, indicating the presence of surface membrane channels (Fig. 6 a, labeled Q). The duration of the activating pulse was chosen to accommodate the ultra-slow activation of $Ca_V1.1$, but the tail currents (I_{tail}) elicited at 0 mV after this activation pulse were comparatively small. Moreover, blockade of ionic currents revealed both ON gating current, in response to a depolarizing pulse, and OFF gating current during repolarization (Fig. 6 b). Computing I_{tail}/q_{rev} demonstrated low saturating values consistent with a diminished baseline $P_{O,max}$ of $Ca_V1.1$ channels (Fig. 6 c). Moreover, normalized ON and OFF gating charges plotted as a function of voltage overlays on each other demonstrated that Q_{ON} and Q_{OFF} were similar in magnitude and voltage dependence (Figs. 6 d and S2 c). In contrast, with CaM or β_{2A}-CaM coexpressed, $Ca_V1.1$ produce markedly enhanced I_{tail} (Fig. 6, e and i) with similar gating currents (Fig. 6, f and j). Further analysis shows that the saturating value of I_{tail}/q_{rev} is approximately fivefold enhanced in the presence of CaM (Fig. 6 g, P = 0.006) or β_{2A}-CaM (Fig. 6 k, P = 0.004), suggesting that CaM up-regulates $P_{O,max}$. Reassuringly, normalized Q_{ON} and Q_{OFF} were similar in magnitude in the presence of CaM and β_{2A}-CaM (Fig. 6, h and l). In like manner, overexpression of stac3 also resulted in enhanced I_{tail}/q_{rev} (P = 0.006) for $Ca_V1.1$ (Fig. 6, m–p). These results indicate that both CaM and stac up-regulate the maximal P_O of $Ca_V1.1$ (Fig. 6 q). Reassuringly, further quantification of gating charge density at +80 mV ($Q_{density}$[+80]) showed a significant increase for β_{2A}-CaM (P = 0.039) and stac3 (P = 0.045), confirming that modulatory agents also enhance trafficking of $Ca_V1.1$ to the plasma membrane (Fig. 6 r). Together, these data suggest that both modulators not only boost surface–membrane expression but also up-regulate the activity of $Ca_V1.1$. The CaM-dependent change in maximal P_O is reminiscent of findings with related $Ca_V1.3$ channels (Adams et al., 2014).

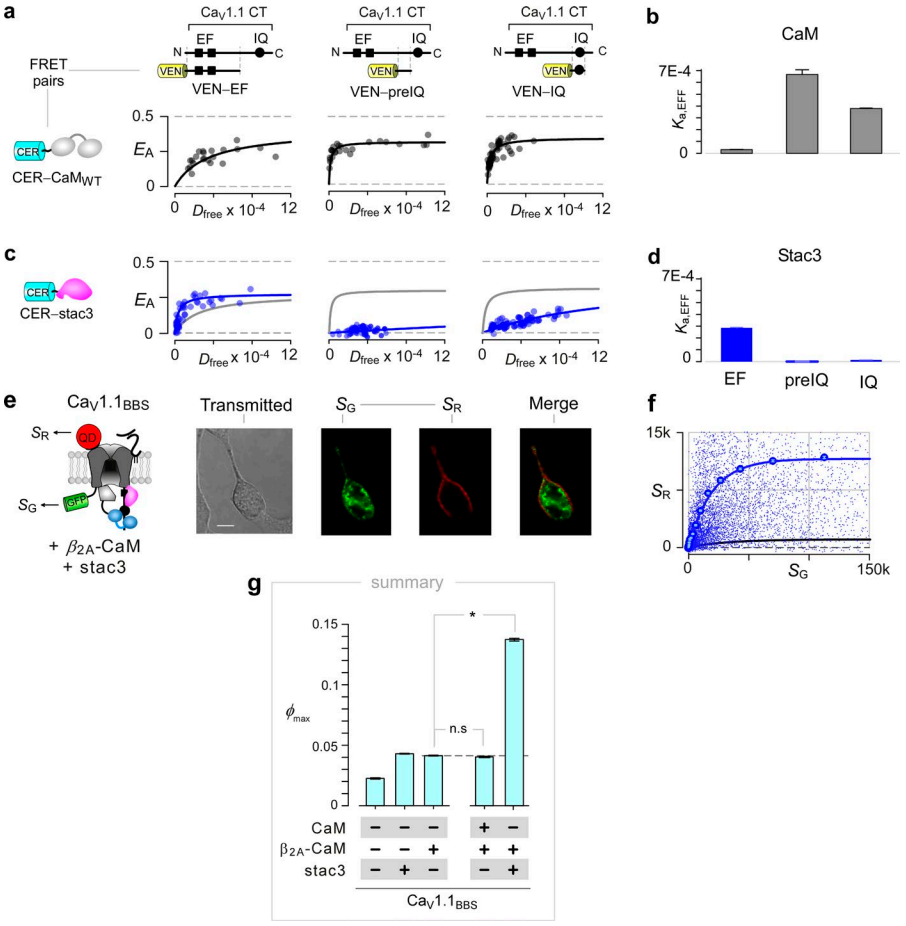

Figure 5. **CaM and stac3 bind to distinct sites on the CT and exert independent trafficking effects. (a)** FRET binding of Ca^{2+}/CaM with EF hands (left), pre-IQ domain (middle), and IQ domain (right) shows weak binding for EF hands and strong binding for pre-IQ and IQ domains. **(b)** Bar graph summary of binding affinities from a. **(c and d)** Stac3 binds preferentially to EF hands. Format as in a and b. **(e and f)** Coexpression of CaM and stac3 results in distinct extracellular labeling and supralinear increase of channels on the membrane. Format as in Fig. 2 (b and c). Bar, 5 µm. **(g)** Bar graph summarizing ϕ_{max} for CaM and stac3 separately as well as together. Expressing CaM and β_{2A}-CaM does not appreciably change ϕ_{max}. In comparison, coexpression of β_{2A}-CaM with stac3 results in a sixfold increase in ϕ_{max}. *, $P < 10^{-5}$. Error bars show mean ± SEM.

Myopathy-associated stac3 mutants diminish $Ca_V1.1$ surface–membrane trafficking

Recent genetic screens have identified multiple mutations within stac3 that are associated with severe congenital myopathies as illustrated in Fig. 7 a. The first autosomal recessive mutation observed in patients of the Lumbee Native American tribe were homozygous autosomal recessive (W[284]S) in the first SH3 domain of stac3 (Stamm et al., 2008). Subsequently, compound heterozygous variants (K[288]* and L[111]Δ) were identified in a patient of Turkish heritage (Grzybowski et al., 2017). Given that stac3 binds to the $Ca_V1.1$ CT, we considered whether myopathy-associated mutants may disrupt this interaction and diminish surface–membrane trafficking.

Using a FRET two-hybrid assay, we assessed the binding of Ven-tagged $Ca_V1.1$ CI and Cer-tagged stac3 variants (Fig. 7 b). In comparison with WT, all three disease-associated stac3 variants exhibited a spectrum of weakened binding affinities (Fig. 7 c; black, WT; red, mutant). Stac3 variants L[111]Δ and W[284]S showed a nearly 10-fold weakened affinity, whereas the mutation K[288]* resulted in a twofold reduced binding of $Ca_V1.1$ carboxy terminus (Fig. 7 j). To discern analogous functional changes, we compared the surface–membrane trafficking of $Ca_V1.1_{BBS}$ with WT or mutant stac3 in the presence of both β_{1A} and $\alpha_2\delta$ subunits. Upon coexpression of WT stac3, $Ca_V1.1_{BBS}$ showed strong QD labeling, confirmed by confocal imaging (Fig. 7 d) and flow cytometric analysis (Fig. 7, e and k), suggesting robust surface–membrane expression. In contrast, coexpression of stac3 variant W[284]S with $Ca_V1.1_{BBS}$ resulted in sharply diminished QD labeling visualized via confocal imaging (Fig. 7 f). Population analysis using flow cytometric analysis further confirmed this result ($P < 10^{-5}$; Fig. 7, g and k). Likewise, analysis of two additional disease-associated stac3 variants, L[111]Δ ($P < 10^{-5}$) and K[288]* ($P < 10^{-5}$), revealed variably diminished channel surface–membrane trafficking as evident from reduced ϕ_{max} (Fig. 7 k). Quantitatively, if the binding of stac3 to $Ca_V1.1_{BBS}$ genuinely underlies the enhancement in channel surface–membrane trafficking, then this functional increase will follow a Langmuir function with the binding affinity of the stac–channel interaction as follows:

$$\phi_{max}^{stac3} = \phi_{max}^{baseline} + \varphi_{stac3} \cdot \frac{K_a}{K_a + \Lambda}, \quad (6)$$

where ϕ_{stac3} and Λ are constants and ϕ_{max}^{stac3} and $\phi_{max}^{baseline}$ represent the saturating surface–membrane trafficking limit in the presence and absence of stac3, respectively (see supplemental text). For stac3 variants, we assume that their relative binding affinity for the $Ca_V1.1$ CI deduced from FRET two-hybrid binding assays ($K_{a,EFF}$) is proportional to that for the holochannel interface (K_a). This theoretical framework for channel trafficking mirrors individually transformed Langmuir analysis previously developed to deduce binding interfaces critical for channel gating (Ben Johny et al., 2013). Plotting the experimentally determined saturating surface–membrane trafficking ratio ϕ_{max} versus the relative $Ca_V1.1$ CI binding affinities ($K_{d,EFF}$) for the stac3 variants reveals the predicted Langmuir relationship (Fig. 7 l). These results

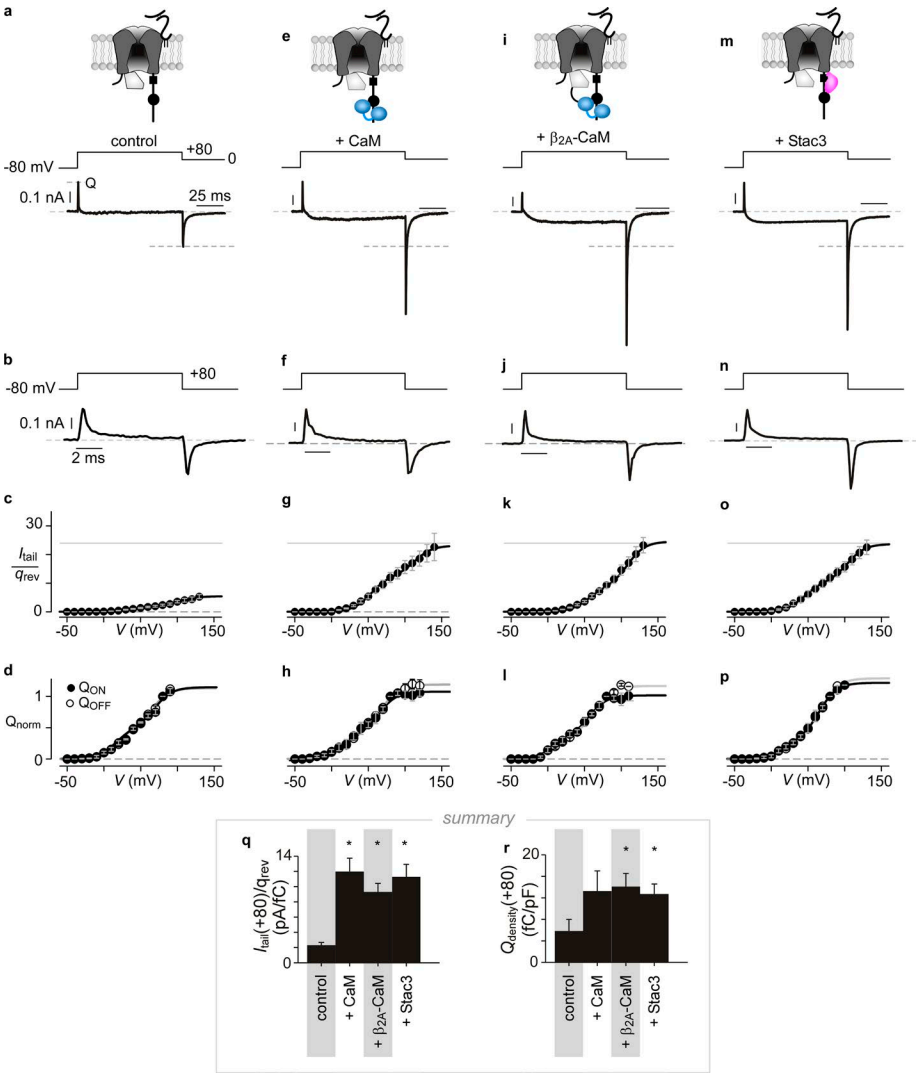

Figure 6. ***P*$_O$ of Ca$_V$1.1 is increased with CaM and stac3. (a)** Ca$_V$1.1 with only its auxiliary β_{2A} and $\alpha_2\delta$ subunits elicits small tail current (I_{tail}) despite large gating charge movement, indicating a low P_O for these channels at baseline. Top: Cartoon depicts Ca$_V$1.1 α_1 subunit bound to auxiliary β_{2A} and $\alpha_2\delta$ subunits in HEK293 cells. Bottom: Exemplar currents elicited in response to voltage step depolarization from −80 mV to +80 mV show large gating-charge movement at the reversal potential (q_{rev}) and I_{tail} evoked upon repolarization to 0 mV. **(b)** Exemplar current trace for gating charge movement after pore block with Cd^{2+}/La^{3+} with voltage step depolarization from −80 mV to +80 mV and back to −80 mV. Trace shows equivalent gating charge movement into the open conformation (Q_{ON}) and gating charge movement into the closed conformation (Q_{OFF}). **(c)** Population data reveal low P_O. In this figure, I_{tail} evoked in response to a voltage-step family with varying prepulse potentials is normalized by the gating charge movement at the reversal potential, q_{rev}. This ratio (I_{tail}/q_{rev}) is proportional to P_O of the channel. **(d)** Population data of normalized Q_{OFF} to Q_{ON} confirms equivalent charge movement and also the reliability for approximating P_O. **(e–h)** Overexpression of CaM enhances the ratio of I_{tail}/q_{rev}, arguing that CaM enhances baseline P_O of Ca$_V$1.1. Format as in a–d. **(i–l)** Similarly, localized delivery of CaM via fusion to the β_{2A} subunit enhances I_{tail} despite similar q_{rev}. Format as in a–d. **(m–p)** Coexpression of stac3 also increases I_{tail}/q_{rev} by approximately fivefold, which is comparable with CaM. Format as in a–d. **(q)** Population data of I_{tail} (+80 mV)/q_{rev} show significant increase of P_O with the addition of CaM or stac3. *, $P < 0.01$. **(r)** Population data of $Q_{density}$ (+80 mV) confirm increase of channels on the membrane with the addition of CaM or stac3. *, $P < 0.05$. Black bars indicate mean ± SEM. Gray shaded boxes are visual guides for comparison across conditions.

demonstrate that stac3 binding to Ca$_V$1.1 promotes plasmalemmal trafficking and that myopathy-associated stac variants exhibit weakened trafficking resulting from disrupted binding to the Ca$_V$1.1 CT.

Given that both CaM and stac3 independently enhance surface–membrane trafficking of Ca$_V$1.1, we next investigated whether CaM might rescue the defects in trafficking associated with myopathy-associated stac3. Consequently, we assessed surface–membrane trafficking of Ca$_V$1.1$_{BBS}$ in the presence of both stac3 W[284]S and CaM$_{WT}$. Confocal imaging showed an increase in QD labeling (Fig. 7 h), and flow cytometry confirmed a modest rescue at the population level ($P < 10^{-5}$; Fig. 7 i). Similar analysis with other myopathy-associated stac3 variants (L[111]Δ and K[288]*) further confirmed the partial rescue of Ca$_V$1.1$_{BBS}$ trafficking when CaM$_{WT}$ is coexpressed ($P < 10^{-5}$ for both variants; Fig. 7 k). Intriguingly, the net magnitude of CaM-dependent enhancement in Ca$_V$1.1 surface–membrane trafficking is similar in the presence of all stac3 variants irrespective of their binding affinities (Fig. S3). These results suggest that the CaM effect on channel trafficking is independent of stac, consistent with the two regulatory proteins using distinct binding interfaces (Fig. S3), and raise the possibility that CaM delivery to Ca$_V$1.1 furnishes an orthogonal strategy for partially reversing functional defects resulting from myopathy-associated mutations in stac3. Moreover, Ca$_V$1.1 CT represents a prime interface for screening small molecules that promote Ca$_V$1.1 trafficking and function.

Small-molecule modulators reverse myopathy-associated Ca$_V$1.1 trafficking defects

Recently, pharmacological chaperones have emerged as a promising strategy to rescue surface–membrane trafficking deficits observed in a variety of genetic disorders involving both G protein–coupled receptors (Beerepoot et al., 2017) and ion channels such as cystic fibrosis transmembrane conductance regulator associated with cystic fibrosis (Hanrahan et al., 2013), K_{ATP} channels associated with congenital hyperinsulinism of infancy (Martin et al., 2013), and Na$_V$1.5 channels associated with Brugada syndrome (Valdivia et al., 2004; Moreau et al., 2012). In many of these cases, small-molecule modulators that alter channel gating may offer a dual purpose as chaperones

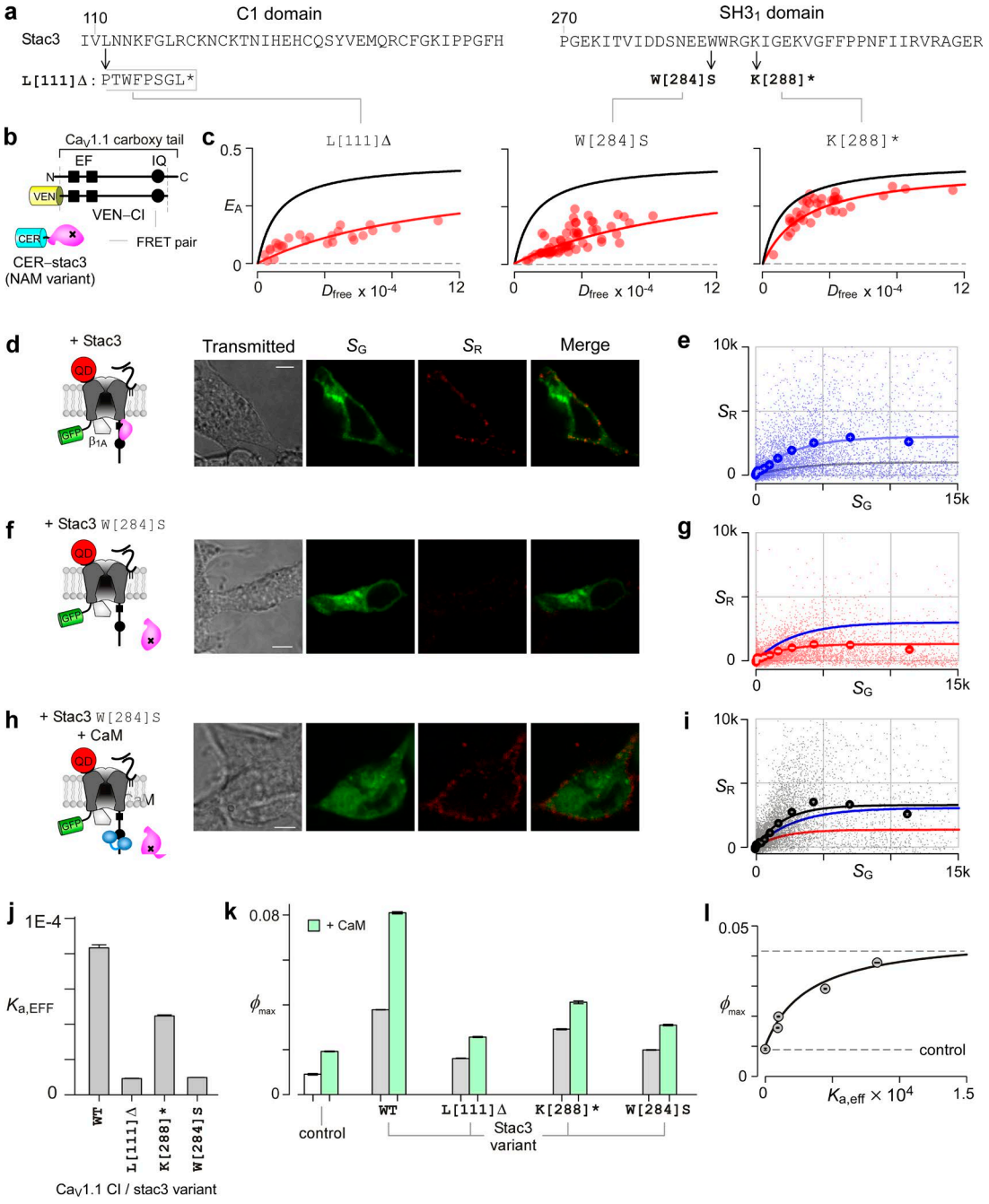

Figure 7. **Myopathic stac3 mutations reduce binding to the CT and surface membrane trafficking. (a)** Amino acid sequence for stac3 mutations in both the C1 and first SH3 domain (SH3$_1$). **(b)** Schematic shows fluorophore-tagged FRET pairs, Ven-CI of Ca$_V$1.1 with Cer-tagged stac3 variants. NAM, Native American myopathy. **(c)** Myopathy-associated stac3 variants weaken binding to Ca$_V$1.1 CI. Left: Intron insert results in a frameshift, and truncation of SH3 domains (L[111]Δ) dramatically reduces stac3 binding to Ca$_V$1.1 CI. Middle: A point mutation in the first SH3 domain (W[284]S) strongly reduces stac3 binding. Right: Disease-associated stac3 variant with a nonsense mutation in the second SH3 domain (K[288]*) moderately weakens binding to Ca$_V$1.1. **(d)** Stac3 strongly enhances Ca$_V$1.1 surface–membrane trafficking in the presence of β$_{1A}$ and α2δ subunits as demonstrated by detectible BTX labeling in exemplar confocal images. Format as in Fig. 2 b. **(e)** Flow cytometric analysis confirms high expression of Ca$_V$1.1 when bound to stac3. Format as in Fig. 2 c. **(f and g)** Coexpression of myopathy-associated stac3 mutant (W[284]S) results in only modest enhancement in Ca$_V$1.1 surface–membrane trafficking as illustrated by confocal imaging and flow cytometry. Format as in d and e, respectively. **(h and i)** Coexpression of CaM with mutant stac3 (W[284]S) results a large increase of Ca$_V$1.1 surface membrane trafficking comparable with that with WT stac3. Format as in d and e. Bars, 5 µm. **(j)** Bar graph summarizes binding affinities of stac variants to Ca$_V$1.1 CI, mean ± SEM. **(k)** Bar graph summarizes the saturating surface–membrane trafficking limit ϕ_{max} of Ca$_V$1.1 in the presence of myopathy-associated mutant stac3 and corresponding rescue with CaM. Stac3 mutations that weaken binding to Ca$_V$1.1 CT also reduce surface–membrane trafficking (gray bar) and may be partially rescued with CaM coexpression (green bar). Control (white) bar is Ca$_V$1.1 expressed with basic auxiliary subunits α$_2$δ and β$_{1A}$ for comparison. **(l)** For all stac3 variants, plotting ϕ_{max} versus the association constant ($K_{a,EFF}$ = 1/$K_{d,EFF}$; d) for the binding of mutant stac3 to Ca$_V$1.1 CI module reveals a Langmuir relationship, suggesting that the binding of stac3 is a key determinant for Cav1.1 surface–membrane trafficking. Dashed gray lines are the ϕ_{max} for with (top) and without (bottom) stac3$_{WT}$.

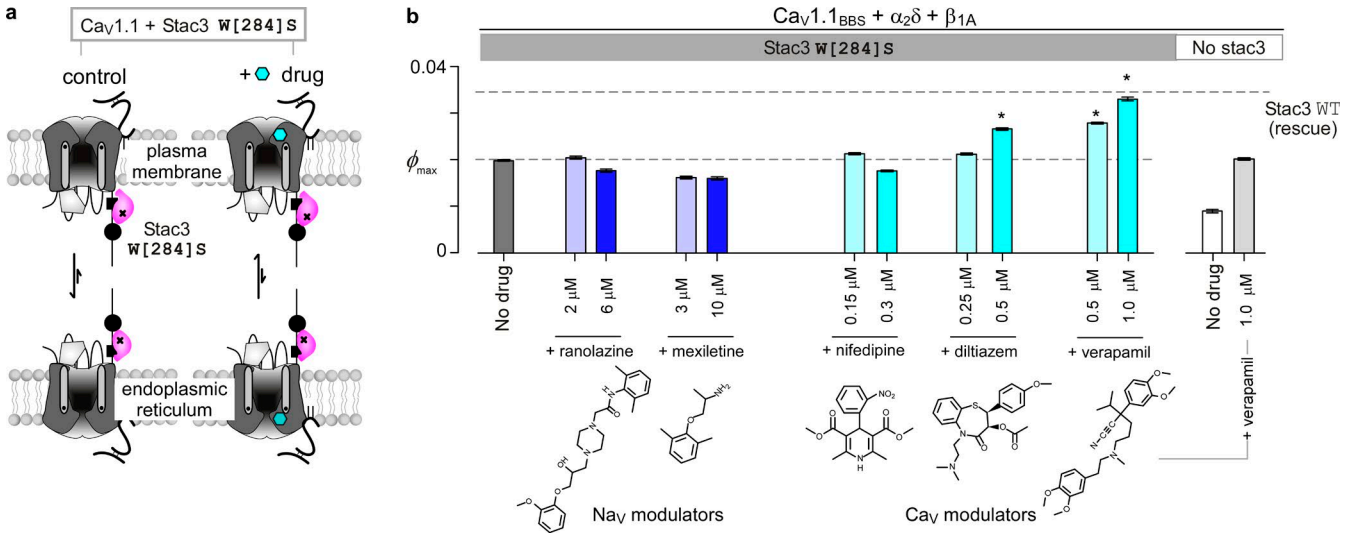

Figure 8. **Small-molecule modulators partially rescue pathological deficits in $Ca_V1.1$ trafficking. (a)** Cartoon shows potential enhancement of $Ca_V1.1$ plasmalemmal trafficking in the presence of potential pharmacological agents. Left: $Ca_V1.1$, when bound to myopathy-associated mutant stac3 (W[284]S) and $\alpha_2\delta$ and β_{1A} subunits, traffics poorly to the plasma membrane. Right: Addition of a small-molecule trafficking modulator may enhance the fraction of surface–membrane channels. **(b)** Bar graph summarizes changes in the saturating surface–membrane trafficking limit (ϕ_{max}) of $Ca_V1.1$ trafficking after addition of various small-molecule modulators at low and high concentrations. Bottom dashed line corresponds with baseline trafficking with myopathic stac3 (W[284]S; gray); top dashed line corresponds with $Ca_V1.1$ trafficking with WT stac3. Both diltiazem and verapamil markedly enhanced ϕ_{max}, whereas dihydropyridines and Na channel modulators ranolazine and mexiletine did not substantially alter $Ca_V1.1$ trafficking. Without stac3, 1 μM verapamil increased $Ca_V1.1$ trafficking by approximately twofold (*, $P < 10^{-5}$). Error bars show mean ± SEM.

by stabilizing key channel conformations. Moreover, as Ca^{2+} influx through $Ca_V1.1$ channels is not necessary to trigger muscle contraction (Armstrong et al., 1972; Dayal et al., 2017), we reasoned that clinically relevant small-molecule Ca_V1 antagonists that traditionally block Ca^{2+} influx may be repurposed to reverse trafficking defects of $Ca_V1.1$ observed in the presence of myopathy-associated mutant stac3 (Fig. 8 a). To evaluate this possibility, bungarotoxin-labeling assays and flow-cytometric analysis were used to quantify drug-induced changes in $Ca_V1.1$ trafficking coexpressed with mutant stac3 W[284]S, the most prevalent myopathy-associated stac variant, and $\alpha_2\delta$ and β_{1A} auxiliary subunits. We tested three L-type Ca^{2+}-channel modulators, nifedipine, diltiazem, and verapamil (Fig. 8 b, cyan bars), as well as two Na channel modulators, mexiletine and ranolazine (Fig. 8 b, blue bars), clinically approved for various cardiovascular conditions, at two concentrations reflecting typical low and high therapeutic plasma concentrations. Remarkably, among Ca_V channel modulators, incubation with verapamil resulted in ∼40% recovery of $Ca_V1.1$ trafficking (Fig. 8 b) at low (>60%) drug concentration and ∼67% recovery at high (>80%) drug concentration ($P < 10^{-5}$). Diltiazem also increased channel trafficking by ∼34% at high (>80%) drug concentration ($P < 10^{-5}$). In contrast, incubation with nifedipine, mexiletine, and ranolazine resulted in minimal change (<10%) in the saturating fraction of surface–membrane channels (ϕ_{max}; Fig. 8 b). Of note, in all five conditions, the total GFP fluorescence remained the same, suggesting that the increase in the fraction of surface–membrane channels (ϕ_{max}) observed in the presence of verapamil and diltiazem reflects genuine potentiation of channel plasmalemmal trafficking. Verapamil application increased $Ca_V1.1$ trafficking in the absence of stac3 by approximately twofold (Fig. 8 b) but increased channel trafficking in the presence of CaM and stac3 by only 24% and 33%, respectively (Fig. S4 a). Importantly, as stac3 is also thought to directly mediate EC coupling, the partial rescue of trafficking observed in this study may not suffice to rescue deficits in muscle contraction. Nonetheless, these results highlight the utility of the bungarotoxin-labeling assay for small-molecule screens of pharmacological chaperones.

Discussion

$Ca_V1.1$ has often appeared atypical among L-type channels with seemingly poor conservation of regulatory mechanisms and idiosyncratic requirements for membrane expression manifesting as a loss of function in heterologous systems. Our results indicate that reduced function stems from two deficits. First, quantitative flow-cytometric analyses of surface–membrane expression show that $Ca_V1.1$ with β and $\alpha_2\delta$ subunits traffics to the plasma membrane, albeit at reduced levels in comparison with related L-type channels. Second, electrophysiological analyses reveal that $Ca_V1.1$ exhibits a low P_O. Both deficits in function depend on the channel CT harboring distinct binding interfaces for CaM and stac3, and coexpression of these proteins markedly enhances channel function. In addition, multiple myopathy-associated mutations weaken stac3 binding to $Ca_V1.1$ CT and fail to promote channel trafficking. Further analysis of trafficking demonstrated that clinically used Ca_V1 antagonists verapamil and diltiazem reverse trafficking defects of $Ca_V1.1$. In all, these findings highlight parallel mechanisms that buttress $Ca_V1.1$ function in heterologous expression systems, lend insight into pathophysiological deficits of $Ca_V1.1$ associated with congenital myopathy, and posit pharmacological strategies for rescue of channel function.

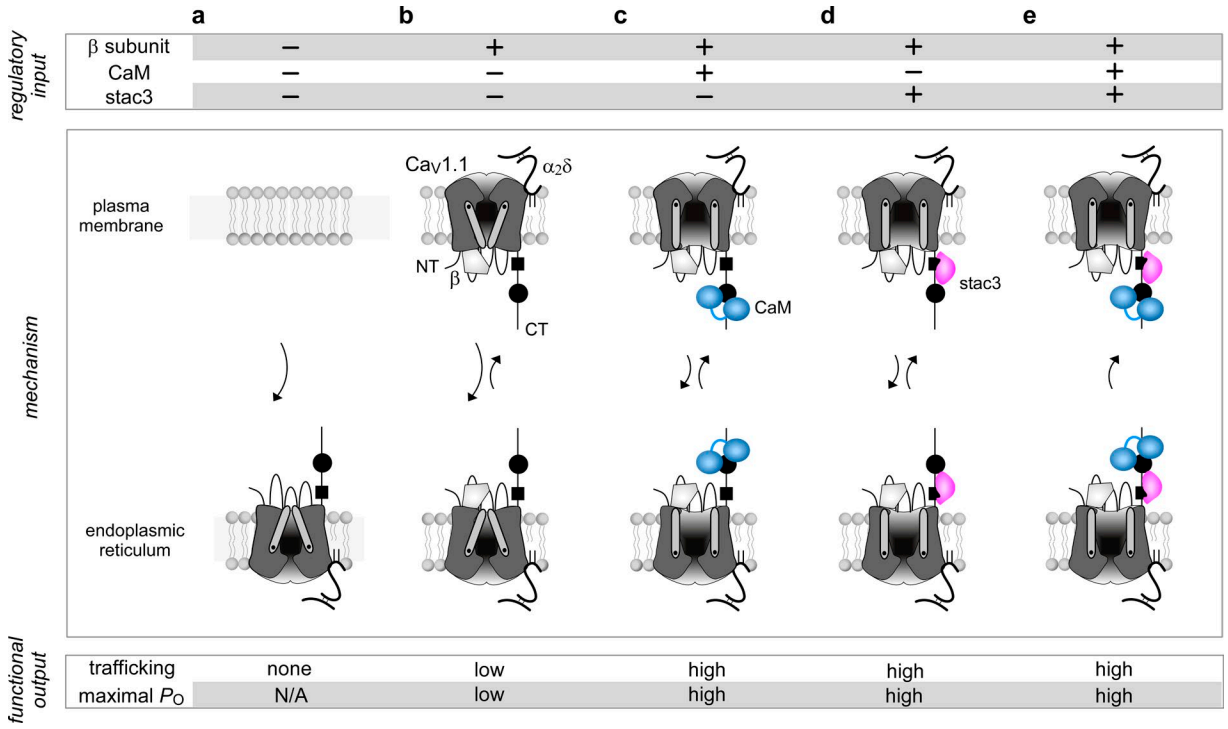

Figure 9. **Molecular determinants for $Ca_V1.1$ functional expression. (a–e)** Schematic illustrates a simplified model for the effect of various regulatory proteins on $Ca_V1.1$ functional expression. For all panels, top and bottom rows identify the regulatory input and functional outcomes, respectively. Middle row schematizes underlying molecular mechanism. **(a)** Devoid of a β subunit, $Ca_V1.1$ fails to traffic to the surface membrane, presumably because of ER retention motifs. **(b)** Binding of the β subunit enables low basal $Ca_V1.1$ surface–membrane trafficking. Channels at the plasma membrane feature a low P_O. **(c)** CaM enhances $Ca_V1.1$ surface–membrane trafficking. The same CaM also enhances baseline P_O. **(d)** Stac3 binding also enhances $Ca_V1.1$ surface–membrane trafficking and up-regulates baseline P_O. **(e)** Binding of CaM and stac allows for high $Ca_V1.1$ trafficking. The channels are presumed to retain a high baseline P_O.

Molecular determinants for $Ca_V1.1$ trafficking in heterologous systems

The requirements for $Ca_V1.1$ surface–membrane trafficking in heterologous systems have long evaded consensus. Although related $Ca_V1/2$ channels exhibit robust plasmalemmal trafficking with β and $\alpha_2\delta$ subunits, additional components such as cytosolic stac3 and the transmembrane γ_1 subunit are thought to be obligatory for $Ca_V1.1$ currents in heterologous systems (Tuluc et al., 2009; Bannister and Beam, 2013; Polster et al., 2015, 2016). How do these modifications at disparate channel interfaces influence trafficking? Our results point to a unified trafficking scheme (Fig. 9), with the requirements for $Ca_V1.1$ trafficking paralleling those for related Ca_V channels (Fang and Colecraft, 2011). Specifically, the β subunit is a dominant effector necessary for $Ca_V1.1$ plasmalemmal trafficking (Fig. 9 a). This requirement of β subunits for $Ca_V1.1$ trafficking fits well with the reduced channel expression and diminished tetrad formation observed in β_{1A}-KO mice (Schredelseker et al., 2005). Upon binding the β subunit, however, $Ca_V1.1$ exhibits only low baseline trafficking (Fig. 9 b). The binding of either CaM or stac3 alone leads to only a partial enhancement in membrane trafficking (Fig. 9, c and d). Finally, the binding of both CaM and stac3 to the $Ca_V1.1$ CT yields a supralinear increase in membrane trafficking (Fig. 9 e). Interestingly, complete removal of the CT results in a basal increase in channel trafficking, suggesting that there may be retention motifs encoded within the CT that are masked upon the interaction of either stac3 or CaM (Fig. 4 f). This simplified scheme captures the experimentally observed effects of stac3 and CaM on $Ca_V1.1$ and provides a platform for other indirect mechanisms to be assessed.

Mechanistically, the $Ca_V1.1$ CT is a critical determinant for surface–membrane trafficking by harboring both CaM and stac3, a finding that resonates with early research that identified a vital role for this domain in triad localization (Flucher et al., 2000). As CaM is enriched in the triad via transient association with cytoplasmic loops of RYR1 (Mochca et al., 2001; Sencer et al., 2001; Xiong et al., 2002), its weak binding to $Ca_V1.1$ may promote colocalization of the channels at the tubular or surface membranes (Rodney and Schneider, 2003). Recurrent large-amplitude Ca^{2+} transients in the triadic space may further reinforce this localization. Indeed, the role of Ca^{2+}/CaM in mediating activity-dependent trafficking has emerged as a pervasive theme in Ca_V channel physiology, yet the precise motifs that orchestrate this phenomenon are yet to be elucidated (Wang et al., 2007; Hall et al., 2013; Tseng et al., 2017). Similarly, our results indicate that stac3 potentiates $Ca_V1.1$ trafficking also via interaction with the CT. Even so, CaM and stac3 likely act through distinct sites as their combination supraadditively enhanced channel trafficking. In this regard, recent studies have shown that multiple channel segments including the II–III loop could bind stac3 (Wong King Yuen et al., 2017; Polster et al., 2018), although with weak affinity. It is possible that stac3 interaction with multiple $Ca_V1.1$ segments may concurrently enhance its affinity. Analysis of $stac3^{-/-}$ zebrafish and mouse skeletal myotubes revealed a partial reduction of $Ca_V1.1$ at the triad, leading to incomplete

tetrads and a loss of EC coupling (Polster et al., 2015; Linsley et al., 2017a,b). The magnitude of reduction varied between the two models, suggesting that other regulators such as CaM may play a role in channel trafficking in the muscle. As various stac isoforms promote trafficking of $Ca_V1.2$ and Ca_V3 (Rzhepetskyy et al., 2016), stac may be a shared modulator across the Ca_V family (Weiss and Zamponi, 2017). Our quantitative framework and flow-cytometric analysis of external-epitope labeling may delineate vital signals for membrane trafficking of Ca_V channels in skeletal muscle and other native cell types.

CaM and stac3 modulate channel gating

The ability to resolve $Ca_V1.1$ currents in heterologous systems in the presence of β and $\alpha_2\delta$ subunits alone enables systematic analysis of channel gating modulation by regulatory partners. For nearly all $Ca_V1/2$ channels, CaM confers a potent feedback mechanism (Halling et al., 2006; Minor and Findeisen, 2010; Ben-Johny et al., 2015). Our analysis shows that local enrichment of CaM to $Ca_V1.1$ results in a fivefold increase in maximal P_O (Fig. 6 k). As potentiation in gating occurs at high voltages where channels convey minimal Ca^{2+} influx, this effect likely depends on apoCaM interaction. Excitingly, these results are evocative of recent findings that apoCaM binding augments the baseline P_O of $Ca_V1.3$ variants (Adams et al., 2014), hinting at a conserved mechanism across the Ca_V superfamily (Ben-Johny et al., 2015). Of note, effects on channel gating and trafficking were both elicited by CaM fused to β subunit. As β subunits have a 1:1 stoichiometry with α subunits (Dalton et al., 2005; Wu et al., 2016), a single CaM mediates both functional effects. Thus, CaM signaling may be bifurcated, whereby the apo form enhances channel gating and the Ca^{2+}-bound form enriches channels at the plasma membrane.

Stac3 coexpression up-regulates the baseline P_O of $Ca_V1.1$ to the same extent as CaM depending on the CI module (Fig. 6 o). Interestingly, in skeletal myotubes, homozygous stac3 KO (Polster et al., 2015; Linsley et al., 2017a) and $Ca_V1.1$ mutants with weakened CaM binding (Stroffekova, 2011) lead to a dramatic loss of EC coupling despite the presence of gating charge movements. Thus, robust EC coupling may require a permissive $Ca_V1.1$ CT conformation along with that for the II–III loop (Tanabe et al., 1990a). Synthesizing a general framework of Ca_V modulation by CaM and stac is an exciting frontier, and the ability to express $Ca_V1.1$ in heterologous systems under a wide range of conditions facilitates this pursuit.

Pathophysiology and treatment of myopathy-associated stac mutants

Stac3 has been identified as a vital genetic locus for debilitating congenital myopathy that encompasses an expanding list of mutations. Patients exhibit a plethora of myopathy-associated symptoms including facial weakness with ptosis, hypotonia, small stature, scoliosis, cleft palate, and susceptibility to malignant hyperthermia (Stamm et al., 2008; Zaharieva et al., 2014; Grzybowski et al., 2017; Telegrafi et al., 2017). Current treatment strategies focus on early diagnosis and symptom management, particularly anticipatory management of malignant hyperthermia, and novel small-molecule agents that reverse pathogenesis are highly desired.

Our analysis reveals that disease-associated stac3 variants weaken binding to the CT, resulting in variably diminished $Ca_V1.1$ surface–membrane trafficking, highlighting potential pathogenic mechanisms. Indeed, reconstitution of myopathy-associated mutant stac3 (W[284]S) in $stac3^{-/-}$ KO zebrafish and mouse models led to diminished trafficking, triadic organization, and activity of $Ca_V1.1$, resulting in marked loss of EC coupling (Polster et al., 2016; Linsley et al., 2017a,b). As patients are either homozygous or compound heterozygous for stac mutations, it is likely that the weakened affinity of stac3 for $Ca_V1.1$ CT results in incomplete saturation of $Ca_V1.1$ by this regulatory protein. Our findings point to three distinct avenues for developing effective pharmacological strategies. First, given that CaM can both partially rescue reduced $Ca_V1.1$ trafficking and enhance $Ca_V1.1$ activation gating, local enrichment of CaM may be an effective strategy for reversing the pathophysiology of stac3-associated myopathies. In this regard, a CRISPR-interference approach was recently developed to selectively manipulate CaM expression for a subset of cardiac arrhythmogenic long-QT syndrome (Limpitikul et al., 2017). Second, as we identify $Ca_V1.1$ CT as the primary effector interface for stac3, FRET two-hybrid binding assay may be repurposed to devise high-throughput screens for small-molecule modulators that enhance this interaction and tune skeletal muscle function (Janzen, 2014). Third, certain Ca_V channel antagonists such as diltiazem and verapamil at low therapeutic plasma concentrations partially rescue these trafficking defects, depending on continual exposure to the drug. Structurally, phenylalkylamines such as verapamil bind pore-lining residues of the domain III–IV S6 segments adjacent to the beginning of the carboxy terminus (Striessnig et al., 1990; Tang et al., 2016). Moreover, mutations within the CaM-binding IQ domain in the Ca_V1 carboxy terminus have been shown to allosterically modify binding of phenylalkylamines and other Ca channel antagonists (Dilmac et al., 2004; Huang et al., 2013). Thus, it is possible that the binding of verapamil may either directly stabilize the CT or allosterically switch its conformation to ultimately promote plasmalemmal trafficking. As EC coupling in skeletal muscle does not depend on freely diffusing Ca^{2+} ions, blockade of Ca^{2+} influx resulting from Ca_V antagonists may not significantly alter the strength of EC coupling (Dayal et al., 2017). Paradoxically, recent research has shown that verapamil can potentiate contractions in mouse skeletal muscle (Dayal et al., 2017). Nonetheless, as stac3 is thought to be directly involved in EC coupling, a simple rescue of plasmalemmal channels may be insufficient to reverse pathogenesis in the case of congenital myopathies. Further functional analysis of EC coupling in stac3 mutant animal models after long-term application of verapamil is necessary to assess therapeutic potential. Nonetheless, the quantitative flow-cytometric assay promises to facilitate discovery of small-molecule trafficking modulators. Indeed, similar pharmacological chaperones have emerged as a potential therapeutic avenue for rescue of trafficking deficits associated with cystic fibrosis (Hanrahan et al., 2013), congenital hyperinsulinism of infancy (Martin et al., 2013), and Brugada syndrome (Valdivia et al., 2004; Moreau et al., 2012).

In all, our results hint at a conserved mechanism by which multiple signaling molecules tune $Ca_V1.1$ gating and localization, inform on mechanisms of disease pathogenesis for congenital

myopathy, and suggest potential avenues for development of therapeutic strategies.

Acknowledgments

We thank Dr. Gordon Tomaselli and Dr. Ivy E. Dick for helpful comments on experimental design and the manuscript. We are also grateful for insightful discussions from the Calcium Signals Laboratory. Finally, we could not have completed this work without the inspirational example of our late mentor David T. Yue, who taught us to pursue science with a passion for the truth.

This work was supported by grants from the National Institute of Neurological Disorders and Stroke (grant NS085074 to D.T. Yue and T. Inoue), the National Institute of Mental Health (grant MH065531 to D.T. Yue and M. Ben-Johny), and the National Science Foundation (J. Niu).

The authors declare no competing financial interests.

Author contributions: J. Niu, M. Ben-Johny, D.T. Yue, and T. Inoue conceived and designed the study. J. Niu made the constructs and collected electrophysiological and FRET data with assistance from M. Ben-Johny and W. Yang. J. Niu and W. Yang performed bungarotoxin labeling and flow cytometry experiments. J. Niu and M. Ben-Johny analyzed all data. J. Niu and M. Ben-Johny wrote the manuscript with input from T. Inoue.

Richard W. Aldrich served as editor.

Submitted: 22 January 2018
Revised: 23 March 2018
Accepted: 11 May 2018

References

Adams, P.J., M. Ben-Johny, I.E. Dick, T. Inoue, and D.T. Yue. 2014. Apocalmodulin itself promotes ion channel opening and Ca(2+) regulation. *Cell.* 159:608–622. https://doi.org/10.1016/j.cell.2014.09.047

Anderson, A.A., X. Altafaj, Z. Zheng, Z.M. Wang, O. Delbono, M. Ronjat, S. Treves, and F. Zorzato. 2006. The junctional SR protein JP-45 affects the functional expression of the voltage-dependent Ca2+ channel Cav1.1. *J. Cell Sci.* 119:2145–2155. https://doi.org/10.1242/jcs.02935

Armstrong, C.M., F.M. Bezanilla, and P. Horowicz. 1972. Twitches in the presence of ethylene glycol bis(β-aminoethyl ether)-N,N′-tetracetic acid. *Biochim. Biophys. Acta.* 267:605–608. https://doi.org/10.1016/0005-2728(72)90194-6

Avila, G., and R.T. Dirksen. 2000. Functional impact of the ryanodine receptor on the skeletal muscle L-type Ca^{2+} channel. *J. Gen. Physiol.* 115:467–480. https://doi.org/10.1085/jgp.115.4.467

Bannister, R.A., and K.G. Beam. 2013. Ca(V)1.1: The atypical prototypical voltage-gated Ca^{2+} channel. *Biochim. Biophys. Acta.* 1828:1587–1597. https://doi.org/10.1016/j.bbamem.2012.09.007

Bannister, R.A., D.C. Sheridan, and K.G. Beam. 2016. Distinct components of retrograde Ca(V)1.1-RyR1 coupling revealed by a lethal mutation in RyR1. *Biophys. J.* 110:912–921. https://doi.org/10.1016/j.bpj.2015.12.031

Beerepoot, P., R. Nazari, and A. Salahpour. 2017. Pharmacological chaperone approaches for rescuing GPCR mutants: Current state, challenges, and screening strategies. *Pharmacol. Res.* 117:242–251. https://doi.org/10.1016/j.phrs.2016.12.036

Ben Johny, M., P.S. Yang, H. Bazzazi, and D.T. Yue. 2013. Dynamic switching of calmodulin interactions underlies Ca2+ regulation of CaV1.3 channels. *Nat. Commun.* 4:1717. https://doi.org/10.1038/ncomms2727

Ben-Johny, M., I.E. Dick, L. Sang, W.B. Limpitikul, P.W. Kang, J. Niu, R. Banerjee, W. Yang, J.S. Babich, J.B. Issa, et al. 2015. Towards a unified theory of calmodulin regulation (calmodulation) of voltage-gated calcium and sodium channels. *Curr. Mol. Pharmacol.* 8:188–205. https://doi.org/10.2174/1874467208666150507110359

Black, D.J., D.B. Halling, D.V. Mandich, S.E. Pedersen, R.A. Altschuld, and S.L. Hamilton. 2005. Calmodulin interactions with IQ peptides from voltage-dependent calcium channels. *Am. J. Physiol. Cell Physiol.* 288:C669–C676. https://doi.org/10.1152/ajpcell.00191.2004

Campiglio, M., and B.E. Flucher. 2017. STAC3 stably interacts through its C1 domain with $Ca_V1.1$ in skeletal muscle triads. *Sci. Rep.* 7:41003. https://doi.org/10.1038/srep41003

Campiglio, M., P. Costé de Bagneaux, N.J. Ortner, P. Tuluc, F. Van Petegem, and B.E. Flucher. 2018. STAC proteins associate to the IQ domain of $Ca_V1.2$ and inhibit calcium-dependent inactivation. *Proc. Natl. Acad. Sci. USA.* 115:1376–1381. https://doi.org/10.1073/pnas.1715997115

Catterall, W.A. 2000. Structure and regulation of voltage-gated Ca2+ channels. *Annu. Rev. Cell Dev. Biol.* 16:521–555. https://doi.org/10.1146/annurev.cellbio.16.1.521

Dalton, S., S.X. Takahashi, J. Miriyala, and H.M. Colecraft. 2005. A single CaVbeta can reconstitute both trafficking and macroscopic conductance of voltage-dependent calcium channels. *J. Physiol.* 567:757–769. https://doi.org/10.1113/jphysiol.2005.093195

Dascal, N., I. Lotan, E. Karni, and A. Gigi. 1992. Calcium channel currents in Xenopus oocytes injected with rat skeletal muscle RNA. *J. Physiol.* 450:469–490. https://doi.org/10.1113/jphysiol.1992.sp019137

Dayal, A., K. Schrötter, Y. Pan, K. Föhr, W. Melzer, and M. Grabner. 2017. The Ca^{2+} influx through the mammalian skeletal muscle dihydropyridine receptor is irrelevant for muscle performance. *Nat. Commun.* 8:475. https://doi.org/10.1038/s41467-017-00629-x

Dilmac, N., N. Hilliard, and G.H. Hockerman. 2004. Molecular determinants of frequency dependence and Ca2+ potentiation of verapamil block in the pore region of Cav1.2. *Mol. Pharmacol.* 66:1236–1247. https://doi.org/10.1124/mol.104.000893

Erickson, M.G., B.A. Alseikhan, B.Z. Peterson, and D.T. Yue. 2001. Preassociation of calmodulin with voltage-gated Ca(2+) channels revealed by FRET in single living cells. *Neuron.* 31:973–985. https://doi.org/10.1016/S0896-6273(01)00438-X

Fang, K., and H.M. Colecraft. 2011. Mechanism of auxiliary β-subunit-mediated membrane targeting of L-type (Ca(V)1.2) channels. *J. Physiol.* 589:4437–4455. https://doi.org/10.1113/jphysiol.2011.214247

Flucher, B.E., N. Kasielke, and M. Grabner. 2000. The triad targeting signal of the skeletal muscle calcium channel is localized in the Cooh terminus of the α_{1S} subunit. *J. Cell Biol.* 151:467–478. https://doi.org/10.1083/jcb.151.2.467

Flynn, R., and C. Altier. 2013. A macromolecular trafficking complex composed of β_2-adrenergic receptors, A-kinase anchoring proteins and L-type calcium channels. *J. Recept. Signal Transduct. Res.* 33:172–176. https://doi.org/10.3109/10799893.2013.782219

Franzini-Armstrong, C., and A.O. Jorgensen. 1994. Structure and development of E-C coupling units in skeletal muscle. *Annu. Rev. Physiol.* 56:509–534. https://doi.org/10.1146/annurev.ph.56.030194.002453

Freise, D., B. Held, U. Wissenbach, A. Pfeifer, C. Trost, N. Himmerkus, U. Schweig, M. Freichel, M. Biel, F. Hofmann, et al. 2000. Absence of the gamma subunit of the skeletal muscle dihydropyridine receptor increases L-type Ca2+ currents and alters channel inactivation properties. *J. Biol. Chem.* 275:14476–14481. https://doi.org/10.1074/jbc.275.19.14476

Golini, L., C. Chouabe, C. Berthier, V. Cusimano, M. Fornaro, R. Bonvallet, L. Formoso, E. Giacomello, V. Jacquemond, and V. Sorrentino. 2011. Junctophilin 1 and 2 proteins interact with the L-type Ca2+ channel dihydropyridine receptors (DHPRs) in skeletal muscle. *J. Biol. Chem.* 286:43717–43725. https://doi.org/10.1074/jbc.M111.292755

Goral, R.O., E. Leipold, E. Nematian-Ardestani, and S.H. Heinemann. 2015. Heterologous expression of NaV1.9 chimeras in various cell systems. *Pflugers Arch.* 467:2423–2435. https://doi.org/10.1007/s00424-015-1709-1

Grzybowski, M., A. Schanzer, A. Pepler, C. Heller, B.A. Neubauer, and A. Hahn. 2017. Novel STAC3 mutations in the first non-Amerindian patient with Native American myopathy. *Neuropediatrics.* 48:451–455.

Hall, D.D., S. Dai, P.Y. Tseng, Z. Malik, M. Nguyen, L. Matt, K. Schnizler, A. Shephard, D.P. Mohapatra, F. Tsuruta, et al. 2013. Competition between α-actinin and Ca^{2+}-calmodulin controls surface retention of the L-type Ca^{2+} channel Ca(V)1.2. *Neuron.* 78:483–497. https://doi.org/10.1016/j.neuron.2013.02.032

Halling, D.B., P. Aracena-Parks, and S.L. Hamilton. 2006. Regulation of voltage-gated Ca2+ channels by calmodulin. *Sci. STKE.* 2006:er1.

Halling, D.B., D.K. Georgiou, D.J. Black, G. Yang, J.L. Fallon, F.A. Quiocho, S.E. Pedersen, and S.L. Hamilton. 2009. Determinants in CaV1 channels

that regulate the Ca2+ sensitivity of bound calmodulin. *J. Biol. Chem.* 284:20041–20051. https://doi.org/10.1074/jbc.M109.013326

Hanrahan, J.W., H.M. Sampson, and D.Y. Thomas. 2013. Novel pharmacological strategies to treat cystic fibrosis. *Trends Pharmacol. Sci.* 34:119–125. https://doi.org/10.1016/j.tips.2012.11.006

Horstick, E.J., J.W. Linsley, J.J. Dowling, M.A. Hauser, K.K. McDonald, A. Ashley-Koch, L. Saint-Amant, A. Satish, W.W. Cui, W. Zhou, et al. 2013. Stac3 is a component of the excitation-contraction coupling machinery and mutated in Native American myopathy. *Nat. Commun.* 4:1952. https://doi.org/10.1038/ncomms2952

Huang, H., D. Yu, and T.W. Soong. 2013. C-terminal alternative splicing of CaV1.3 channels distinctively modulates their dihydropyridine sensitivity. *Mol. Pharmacol.* 84:643–653. https://doi.org/10.1124/mol.113.087155

Janzen, W.P. 2014. Screening technologies for small molecule discovery: The state of the art. *Chem. Biol.* 21:1162–1170. https://doi.org/10.1016/j.chembiol.2014.07.015

Johnson, B.D., J.P. Brousal, B.Z. Peterson, P.A. Gallombardo, G.H. Hockerman, Y. Lai, T. Scheuer, and W.A. Catterall. 1997. Modulation of the cloned skeletal muscle L-type Ca2+ channel by anchored cAMP-dependent protein kinase. *J. Neurosci.* 17:1243–1255. https://doi.org/10.1523/JNEUROSCI.17-04-01243.1997

Lamb, G.D. 2000. Excitation-contraction coupling in skeletal muscle: Comparisons with cardiac muscle. *Clin. Exp. Pharmacol. Physiol.* 27:216–224. https://doi.org/10.1046/j.1440-1681.2000.03224.x

Lambert, R.C., Y. Maulet, J.L. Dupont, S. Mykita, P. Craig, S. Volsen, and A. Feltz. 1996. Polyethylenimine-mediated DNA transfection of peripheral and central neurons in primary culture: Probing Ca2+ channel structure and function with antisense oligonucleotides. *Mol. Cell. Neurosci.* 7:239–246. https://doi.org/10.1006/mcne.1996.0018

Lee, A., T. Scheuer, and W.A. Catterall. 2000. Ca2+/calmodulin-dependent facilitation and inactivation of P/Q-type Ca2+ channels. *J. Neurosci.* 20:6830–6838. https://doi.org/10.1523/JNEUROSCI.20-18-06830.2000

Lee, S.R., L. Sang, and D.T. Yue. 2016. Uncovering aberrant mutant PKA function with flow cytometric FRET. *Cell Reports.* 14:3019–3029. https://doi.org/10.1016/j.celrep.2016.02.077

Liang, H., C.D. DeMaria, M.G. Erickson, M.X. Mori, B.A. Alseikhan, and D.T. Yue. 2003. Unified mechanisms of Ca^{2+} regulation across the Ca^{2+} channel family. *Neuron.* 39:951–960. https://doi.org/10.1016/S0896-6273(03)00560-9

Limpitikul, W.B., I.E. Dick, D.J. Tester, N.J. Boczek, P. Limphong, W. Yang, M.H. Choi, J. Babich, D. DiSilvestre, R.J. Kanter, et al. 2017. A precision medicine approach to the rescue of function on malignant calmodulinopathic long-QT syndrome. *Circ. Res.* 120:39–48. https://doi.org/10.1161/CIRCRESAHA.116.309283

Linsley, J.W., I.U. Hsu, L. Groom, V. Yarotskyy, M. Lavorato, E.J. Horstick, D. Linsley, W. Wang, C. Franzini-Armstrong, R.T. Dirksen, and J.Y. Kuwada. 2017a. Congenital myopathy results from misregulation of a muscle Ca2+ channel by mutant Stac3. *Proc. Natl. Acad. Sci. USA.* 114:E228–E236. https://doi.org/10.1073/pnas.1619238114

Linsley, J.W., I.U. Hsu, W. Wang, and J.Y. Kuwada. 2017b. Transport of the alpha subunit of the voltage gated L-type calcium channel through the sarcoplasmic reticulum occurs prior to localization to triads and requires the beta subunit but not Stac3 in skeletal muscles. *Traffic.* 18:622–632. https://doi.org/10.1111/tra.12502

Liu, X., P.S. Yang, W. Yang, and D.T. Yue. 2010. Enzyme-inhibitor-like tuning of $Ca^{(2+)}$ channel connectivity with calmodulin. *Nature.* 463:968–972. https://doi.org/10.1038/nature08766

Marshall, M.R., J.P. Clark III, R. Westenbroek, F.H. Yu, T. Scheuer, and W.A. Catterall. 2011. Functional roles of a C-terminal signaling complex of CaV1 channels and A-kinase anchoring protein 15 in brain neurons. *J. Biol. Chem.* 286:12627–12639. https://doi.org/10.1074/jbc.M110.175257

Martin, G.M., P.C. Chen, P. Devaraneni, and S.L. Shyng. 2013. Pharmacological rescue of trafficking-impaired ATP-sensitive potassium channels. *Front. Physiol.* 4:386. https://doi.org/10.3389/fphys.2013.00386

McRory, J.E., J. Hamid, C.J. Doering, E. Garcia, R. Parker, K. Hamming, L. Chen, M. Hildebrand, A.M. Beedle, L. Feldcamp, et al. 2004. The CACNA1F gene encodes an L-type calcium channel with unique biophysical properties and tissue distribution. *J. Neurosci.* 24:1707–1718. https://doi.org/10.1523/JNEUROSCI.4846-03.2004

Mikami, A., K. Imoto, T. Tanabe, T. Niidome, Y. Mori, H. Takeshima, S. Narumiya, and S. Numa. 1989. Primary structure and functional expression of the cardiac dihydropyridine-sensitive calcium channel. *Nature.* 340:230–233. https://doi.org/10.1038/340230a0

Minor, D.L. Jr., and F. Findeisen. 2010. Progress in the structural understanding of voltage-gated calcium channel (CaV) function and modulation. *Channels (Austin).* 4:459–474. https://doi.org/10.4161/chan.4.6.12867

Mochca, J.M., P. Pate, J.Z. Zhang, and S.L. Hamilton. 2001. Interaction of carboxy-terminal of the alpha 1 subunit of the skeletal muscle DHPR with the calmodulin binding site on RyR1. *Biophys. J.* 80:379a.

Moreau, A., D.I. Keller, H. Huang, V. Fressart, C. Schmied, Q. Timour, and M. Chahine. 2012. Mexiletine differentially restores the trafficking defects caused by two brugada syndrome mutations. *Front. Pharmacol.* 3:62. https://doi.org/10.3389/fphar.2012.00062

Nakai, J., R.T. Dirksen, H.T. Nguyen, I.N. Pessah, K.G. Beam, and P.D. Allen. 1996. Enhanced dihydropyridine receptor channel activity in the presence of ryanodine receptor. *Nature.* 380:72–75. https://doi.org/10.1038/380072a0

Nelson, B.R., F. Wu, Y. Liu, D.M. Anderson, J. McAnally, W. Lin, S.C. Cannon, R. Bassel-Duby, and E.N. Olson. 2013. Skeletal muscle-specific T-tubule protein STAC3 mediates voltage-induced Ca2+ release and contractility. *Proc. Natl. Acad. Sci. USA.* 110:11881–11886. https://doi.org/10.1073/pnas.1310571110

Obermair, G.J., G. Kugler, S. Baumgartner, P. Tuluc, M. Grabner, and B.E. Flucher. 2005. The Ca2+ channel alpha2delta-1 subunit determines Ca2+ current kinetics in skeletal muscle but not targeting of alpha1S or excitation-contraction coupling. *J. Biol. Chem.* 280:2229–2237. https://doi.org/10.1074/jbc.M411501200

Obermair, G.J., P. Tuluc, and B.E. Flucher. 2008. Auxiliary Ca(2+) channel subunits: Lessons learned from muscle. *Curr. Opin. Pharmacol.* 8:311–318. https://doi.org/10.1016/j.coph.2008.01.008

Ohrtman, J., B. Ritter, A. Polster, K.G. Beam, and S. Papadopoulos. 2008. Sequence differences in the IQ motifs of CaV1.1 and CaV1.2 strongly impact calmodulin binding and calcium-dependent inactivation. *J. Biol. Chem.* 283:29301–29311. https://doi.org/10.1074/jbc.M805152200

Park, C.Y., A. Shcheglovitov, and R. Dolmetsch. 2010. The CRAC channel activator STIM1 binds and inhibits L-type voltage-gated calcium channels. *Science.* 330:101–105. https://doi.org/10.1126/science.1191027

Perez-Reyes, E., H.S. Kim, A.E. Lacerda, W. Horne, X.Y. Wei, D. Rampe, K.P. Campbell, A.M. Brown, and L. Birnbaumer. 1989. Induction of calcium currents by the expression of the alpha 1-subunit of the dihydropyridine receptor from skeletal muscle. *Nature.* 340:233–236. https://doi.org/10.1038/340233a0

Perez-Reyes, E., A. Castellano, H.S. Kim, P. Bertrand, E. Baggstrom, A.E. Lacerda, X.Y. Wei, and L. Birnbaumer. 1992. Cloning and expression of a cardiac/brain beta subunit of the L-type calcium channel. *J. Biol. Chem.* 267:1792–1797.

Perni, S., M. Lavorato, and K.G. Beam. 2017. De novo reconstitution reveals the proteins required for skeletal muscle voltage-induced Ca^{2+} release. *Proc. Natl. Acad. Sci. USA.* 114:13822–13827. https://doi.org/10.1073/pnas.1716461115

Peterson, B.Z., C.D. DeMaria, J.P. Adelman, and D.T. Yue. 1999. Calmodulin is the Ca^{2+} sensor for Ca2+-dependent inactivation of L-type calcium channels. *Neuron.* 22:549–558. https://doi.org/10.1016/S0896-6273(00)80709-6

Pitt, G.S., R.D. Zühlke, A. Hudmon, H. Schulman, H. Reuter, and R.W. Tsien. 2001. Molecular basis of calmodulin tethering and Ca2+-dependent inactivation of L-type Ca2+ channels. *J. Biol. Chem.* 276:30794–30802. https://doi.org/10.1074/jbc.M104959200

Polster, A., S. Perni, H. Bichraoui, and K.G. Beam. 2015. Stac adaptor proteins regulate trafficking and function of muscle and neuronal L-type Ca2+ channels. *Proc. Natl. Acad. Sci. USA.* 112:602–606. https://doi.org/10.1073/pnas.1423113112

Polster, A., B.R. Nelson, E.N. Olson, and K.G. Beam. 2016. Stac3 has a direct role in skeletal muscle-type excitation-contraction coupling that is disrupted by a myopathy-causing mutation. *Proc. Natl. Acad. Sci. USA.* 113:10986–10991. https://doi.org/10.1073/pnas.1612441113

Polster, A., B.R. Nelson, S. Papadopoulos, E.N. Olson, and K.G. Beam. 2018. Stac proteins associate with the critical domain for excitation–contraction coupling in the II–III loop of $Ca_V1.1$. *J. Gen. Physiol.* 150:613–624.

Powell, J.A., L. Petherbridge, and B.E. Flucher. 1996. Formation of triads without the dihydropyridine receptor α subunits in cell lines from dysgenic skeletal muscle. *J. Cell Biol.* 134:375–387. https://doi.org/10.1083/jcb.134.2.375

Qin, N., R. Olcese, M. Bransby, T. Lin, and L. Birnbaumer. 1999. Ca2+-induced inhibition of the cardiac Ca2+ channel depends on calmodulin. *Proc. Natl. Acad. Sci. USA.* 96:2435–2438. https://doi.org/10.1073/pnas.96.5.2435

Ríos, E., G. Pizarro, and E. Stefani. 1992. Charge movement and the nature of signal transduction in skeletal muscle excitation-contraction coupling. *Annu. Rev. Physiol.* 54:109–133. https://doi.org/10.1146/annurev.ph.54.030192.000545

Rodney, G.G., and M.F. Schneider. 2003. Calmodulin modulates initiation but not termination of spontaneous Ca2+ sparks in frog skeletal muscle. *Biophys. J.* 85:921–932. https://doi.org/10.1016/S0006-3495(03)74531-7

Rzhepetskyy, Y., J. Lazniewska, J. Proft, M. Campiglio, B.E. Flucher, and N. Weiss. 2016. A $Ca_v3.2$/Stac1 molecular complex controls T-type channel expression at the plasma membrane. *Channels (Austin).* 10:346–354. https://doi.org/10.1080/19336950.2016.1186318

Sang, L., I.E. Dick, and D.T. Yue. 2016. Protein kinase A modulation of CaV1.4 calcium channels. *Nat. Commun.* 7:12239. https://doi.org/10.1038/ncomms12239

Schneider, M.F., and W.K. Chandler. 1973. Voltage dependent charge movement of skeletal muscle: A possible step in excitation-contraction coupling. *Nature.* 242:244–246. https://doi.org/10.1038/242244a0

Schredelseker, J., V. Di Biase, G.J. Obermair, E.T. Felder, B.E. Flucher, C. Franzini-Armstrong, and M. Grabner. 2005. The beta 1a subunit is essential for the assembly of dihydropyridine-receptor arrays in skeletal muscle. *Proc. Natl. Acad. Sci. USA.* 102:17219–17224. https://doi.org/10.1073/pnas.0508710102

Schredelseker, J., A. Dayal, T. Schwerte, C. Franzini-Armstrong, and M. Grabner. 2009. Proper restoration of excitation-contraction coupling in the dihydropyridine receptor beta1-null zebrafish relaxed is an exclusive function of the beta1a subunit. *J. Biol. Chem.* 284:1242–1251. https://doi.org/10.1074/jbc.M807767200

Sekine-Aizawa, Y., and R.L. Huganir. 2004. Imaging of receptor trafficking by using alpha-bungarotoxin-binding-site-tagged receptors. *Proc. Natl. Acad. Sci. USA.* 101:17114–17119. https://doi.org/10.1073/pnas.0407563101

Sencer, S., R.V. Papineni, D.B. Halling, P. Pate, J. Krol, J.Z. Zhang, and S.L. Hamilton. 2001. Coupling of RYR1 and L-type calcium channels via calmodulin binding domains. *J. Biol. Chem.* 276:38237–38241.

Singh, A., D. Hamedinger, J.C. Hoda, M. Gebhart, A. Koschak, C. Romanin, and J. Striessnig. 2006. C-terminal modulator controls Ca^{2+}-dependent gating of $Ca_v1.4$ L-type Ca^{2+} channels. *Nat. Neurosci.* 9:1108–1116. https://doi.org/10.1038/nn1751

Stamm, D.S., A.S. Aylsworth, J.M. Stajich, S.G. Kahler, L.B. Thorne, M.C. Speer, and C.M. Powell. 2008. Native American myopathy: Congenital myopathy with cleft palate, skeletal anomalies, and susceptibility to malignant hyperthermia. *Am. J. Med. Genet. A.* 146A:1832–1841. https://doi.org/10.1002/ajmg.a.32370

Striessnig, J., H. Glossmann, and W.A. Catterall. 1990. Identification of a phenylalkylamine binding region within the alpha 1 subunit of skeletal muscle Ca2+ channels. *Proc. Natl. Acad. Sci. USA.* 87:9108–9112. https://doi.org/10.1073/pnas.87.23.9108

Stroffekova, K. 2008. Ca2+/CaM-dependent inactivation of the skeletal muscle L-type Ca2+ channel (Cav1.1). *Pflugers Arch.* 455:873–884. https://doi.org/10.1007/s00424-007-0344-x

Stroffekova, K. 2011. The IQ motif is crucial for Cav1.1 function. *J. Biomed. Biotechnol.* 2011:504649. https://doi.org/10.1155/2011/504649

Tanabe, T., K.G. Beam, B.A. Adams, T. Niidome, and S. Numa. 1990a. Regions of the skeletal muscle dihydropyridine receptor critical for excitation-contraction coupling. *Nature.* 346:567–569. https://doi.org/10.1038/346567a0

Tanabe, T., A. Mikami, S. Numa, and K.G. Beam. 1990b. Cardiac-type excitation-contraction coupling in dysgenic skeletal muscle injected with cardiac dihydropyridine receptor cDNA. *Nature.* 344:451–453. https://doi.org/10.1038/344451a0

Tang, L., T.M. Gamal El-Din, T.M. Swanson, D.C. Pryde, T. Scheuer, N. Zheng, and W.A. Catterall. 2016. Structural basis for inhibition of a voltage-gated Ca^{2+} channel by Ca^{2+} antagonist drugs. *Nature.* 537:117–121. https://doi.org/10.1038/nature19102

Telegrafi, A., B.D. Webb, S.M. Robbins, C.E. Speck-Martins, D. FitzPatrick, L. Fleming, R. Redett, A. Dufke, G. Houge, J.J.T. van Harssel, et al. Moebius Syndrome Research Consortium. 2017. Identification of STAC3 variants in non-Native American families with overlapping features of Carey-Fineman-Ziter syndrome and Moebius syndrome. *Am. J. Med. Genet. A.* 173:2763–2771. https://doi.org/10.1002/ajmg.a.38375

Tomlinson, W.J., A. Stea, E. Bourinet, P. Charnet, J. Nargeot, and T.P. Snutch. 1993. Functional properties of a neuronal class C L-type calcium channel. *Neuropharmacology.* 32:1117–1126. https://doi.org/10.1016/0028-3908(93)90006-O

Tseng, P.Y., P.B. Henderson, A.C. Hergarden, T. Patriarchi, A.M. Coleman, M.W. Lillya, C. Montagut-Bordas, B. Lee, J.W. Hell, and M.C. Horne. 2017. α-Actinin promotes surface localization and current density of the Ca^{2+} channel $Ca_V1.2$ by binding to the IQ region of the α1 subunit. *Biochemistry.* 56:3669–3681. https://doi.org/10.1021/acs.biochem.7b00359

Tuluc, P., N. Molenda, B. Schlick, G.J. Obermair, B.E. Flucher, and K. Jurkat-Rott. 2009. A CaV1.1 Ca2+ channel splice variant with high conductance and voltage-sensitivity alters EC coupling in developing skeletal muscle. *Biophys. J.* 96:35–44. https://doi.org/10.1016/j.bpj.2008.09.027

Valdivia, C.R., D.J. Tester, B.A. Rok, C.B. Porter, T.M. Munger, A. Jahangir, J.C. Makielski, and M.J. Ackerman. 2004. A trafficking defective, Brugada syndrome-causing SCN5A mutation rescued by drugs. *Cardiovasc. Res.* 62:53–62. https://doi.org/10.1016/j.cardiores.2004.01.022

Wang, H.G., M.S. George, J. Kim, C. Wang, and G.S. Pitt. 2007. Ca2+/calmodulin regulates trafficking of Ca(V)1.2 Ca2+ channels in cultured hippocampal neurons. *J. Neurosci.* 27:9086–9093. https://doi.org/10.1523/JNEUROSCI.1720-07.2007

Wang, Y., X. Deng, S. Mancarella, E. Hendron, S. Eguchi, J. Soboloff, X.D. Tang, and D.L. Gill. 2010. The calcium store sensor, STIM1, reciprocally controls Orai and CaV1.2 channels. *Science.* 330:105–109. https://doi.org/10.1126/science.1191086

Weiss, N., and G.W. Zamponi. 2017. Trafficking of neuronal calcium channels. *Neuronal Signaling.* 1. https://doi.org/10.1042/NS20160003

Wong King Yuen, S.M., M. Campiglio, C.C. Tung, B.E. Flucher, and F. Van Petegem. 2017. Structural insights into binding of STAC proteins to voltage-gated calcium channels. *Proc. Natl. Acad. Sci. USA.* 114:E9520–E9528. https://doi.org/10.1073/pnas.1708852114

Wu, J., Z. Yan, Z. Li, X. Qian, S. Lu, M. Dong, Q. Zhou, and N. Yan. 2016. Structure of the voltage-gated calcium channel Ca(v)1.1 at 3.6 Å resolution. *Nature.* 537:191–196. https://doi.org/10.1038/nature19321

Xiong, L.W., R.A. Newman, G.G. Rodney, O. Thomas, J.Z. Zhang, A. Persechini, M.A. Shea, and S.L. Hamilton. 2002. Lobe-dependent regulation of ryanodine receptor type 1 by calmodulin. *J. Biol. Chem.* 277:40862–40870. https://doi.org/10.1074/jbc.M206763200

Xu, W., and D. Lipscombe. 2001. Neuronal Ca(V)1.3alpha(1) L-type channels activate at relatively hyperpolarized membrane potentials and are incompletely inhibited by dihydropyridines. *J. Neurosci.* 21:5944–5951. https://doi.org/10.1523/JNEUROSCI.21-16-05944.2001

Yang, P.S., B.A. Alseikhan, H. Hiel, L. Grant, M.X. Mori, W. Yang, P.A. Fuchs, and D.T. Yue. 2006. Switching of Ca^{2+}-dependent inactivation of $Ca_{(v)}1.3$ channels by calcium binding proteins of auditory hair cells. *J. Neurosci.* 26:10677–10689. https://doi.org/10.1523/JNEUROSCI.3236-06.2006

Yang, P.S., M.B. Johny, and D.T. Yue. 2014. Allostery in Ca^{2+} channel modulation by calcium-binding proteins. *Nat. Chem. Biol.* 10:231–238. https://doi.org/10.1038/nchembio.1436

Yang, T., X. Xu, T. Kernan, V. Wu, and H.M. Colecraft. 2010. Rem, a member of the RGK GTPases, inhibits recombinant CaV1.2 channels using multiple mechanisms that require distinct conformations of the GTPase. *J. Physiol.* 588:1665–1681. https://doi.org/10.1113/jphysiol.2010.187203

Zaharieva, I.T., I. Colombo, M. Sframeli, J.H. Sigurosson, L. Feng, R. Phadke, C.A. Sewry, J.E. Morgan, and F. Muntoni. 2014. G.P.261: Whole exome sequencing in patients with congenital myopathies. *Neuromuscul. Disord.* 24:895. https://doi.org/10.1016/j.nmd.2014.06.337

Zühlke, R.D., G.S. Pitt, K. Deisseroth, R.W. Tsien, and H. Reuter. 1999. Calmodulin supports both inactivation and facilitation of L-type calcium channels. *Nature.* 399:159–162. https://doi.org/10.1038/20200